



**Rainfall-triggered
deep-seated
landslides**

A. Vallet et al.

This discussion paper is/has been under review for the journal Hydrology and Earth System Sciences (HESS). Please refer to the corresponding final paper in HESS if available.

A new method to compute the groundwater recharge for the study of rainfall-triggered deep-seated landslides. Application to the Séchilienne unstable slope (western Alps)

A. Vallet, C. Bertrand, O. Fabbri, and J. Mudry

CNRS: UMR6249 Chrono-Environnement, Université de Franche-Comté, 16 route de Gray, 25030 Besançon cedex, France

Received: 15 May 2014 – Accepted: 1 June 2014 – Published: 16 June 2014

Correspondence to: A. Vallet (aurelien.vallet@univ-fcomte.fr)

Published by Copernicus Publications on behalf of the European Geosciences Union.

[Title Page](#)

[Abstract](#)

[Introduction](#)

[Conclusions](#)

[References](#)

[Tables](#)

[Figures](#)



[Back](#)

[Close](#)

[Full Screen / Esc](#)

[Printer-friendly Version](#)

[Interactive Discussion](#)



Abstract

Pore water pressure built-up by recharge of underground hydrosystems is one of the main triggering factors of deep-seated landslides. Groundwater recharge, which is the contribution of the precipitation to the recharge of the saturated zone, is a significant parameter. However, in landslide studies, methods and recharge area parameters used to determine the groundwater recharge amount are rarely detailed. Currently, no turnkey method has been proposed to simply and accurately estimate the groundwater recharge. In this study, the groundwater recharge is estimated with a soil–water balance based on characterization of evapotranspiration, soil available water capacity and runoff. Although evapotranspiration estimation is a data-demanding method, many landslide sites have limited meteorological datasets. A workflow method is developed to compute daily groundwater recharge. The method requires only temperature and precipitation as inputs. Soil available water capacity and runoff quantities are determined from field observations and spatial datasets using a spatial composite approach before being refined with a sensitivity analysis. The proposed method is developed to be as versatile as possible in order to be readily applied to other landslide sites, and to be sufficiently simple to be used by any specialist who intends to characterise the relationship between rainfall and landslide displacements. Moreover, this method can be applied to any other parameters, as long as these parameters have a relationship with groundwater recharge. This study demonstrates that, for the Séchilienne landslide, the performance of the correlation between rainfall and displacement is significantly improved with groundwater recharge compared to results obtained with precipitation data.

1 Introduction

Groundwater recharge (hereinafter called recharge) is the part of the precipitation which recharges the saturated zone (aquifer). Patwardhan et al. (1990) showed that the

HESSD

11, 6343–6403, 2014

Rainfall-triggered deep-seated landslides

A. Vallet et al.

Title Page

Abstract

Introduction

Conclusions

References

Tables

Figures



Back

Close

Full Screen / Esc

Printer-friendly Version

Interactive Discussion



**Rainfall-triggered
deep-seated
landslides**

A. Vallet et al.

[Title Page](#)[Abstract](#)[Introduction](#)[Conclusions](#)[References](#)[Tables](#)[Figures](#)[Back](#)[Close](#)[Full Screen / Esc](#)[Printer-friendly Version](#)[Interactive Discussion](#)

soil–water balance method is an accurate way to estimate recharge. Recharge computation with a soil–water balance depends mainly on the surface runoff, the soil available water capacity (SAWC) and the specific vegetation (so-called crop) evapotranspiration (ET_c , also referred as potential evapotranspiration) which is deduced from reference vegetation evapotranspiration (ET_0). The Penman–Monteith method (Allen et al., 1998) is the widely acknowledged standard method to estimate ET_0 . This method requires the knowledge of the relative humidity, the temperature, the wind speed and the solar radiation.

However, most weather stations in landslide areas record only temperature and rainfall. Additionally, solar radiation and relative humidity measurements are subject to drift and inaccuracies leading to bias in evapotranspiration computation (Samani, 2000; Droogers and Allen, 2002). Alternate methods based on empirical or physical equations using a reduced meteorological dataset (reduced-set in short) allow a simpler expression of ET_0 based only on temperature and/or solar radiation (Tabari et al., 2013). Alongside, reduced-set methods have also been developed to estimate solar radiation based on temperature records only (Almorox, 2011). Combination of ET_0 and solar radiation reduced-set methods allow an estimation of ET_0 suitable for landslide analyses by requiring only temperature records. Reduced-set methods were developed under specific site conditions and must be calibrated in order to improve accuracy (Allen et al., 1994; Shahidian et al., 2012).

Pore water pressure built-up by recharge of the aquifer(s) is one of the main triggering factors of motion of deep-seated landslides (Noverraz et al., 1998; Van Asch et al., 1999; Bonzanigo et al., 2001; Guglielmi et al., 2005; Bogaard et al., 2007). In most natural deep-seated landslides, pore water pressure data are not available since piezometers, if any, have a very short lifespan because of slope movements. As a consequence, indirect parameters, such as the calculated recharge, are the only data which enable to understand landslide hydrodynamic behaviour. In this context, recharge is a crucial parameter to estimate.

**Rainfall-triggered
deep-seated
landslides**

A. Vallet et al.

[Title Page](#)[Abstract](#)[Introduction](#)[Conclusions](#)[References](#)[Tables](#)[Figures](#)[Back](#)[Close](#)[Full Screen / Esc](#)[Printer-friendly Version](#)[Interactive Discussion](#)

In most cases, deep-seated landslide studies take into account recharge, either without calibration of the ET_0 reduced-set methods (Binet et al., 2007; Durville et al., 2009; Pisani et al., 2010), or with the use of elaborate or indirect methods (Hong et al., 2005; Cappa et al., 2006; Prokešová et al., 2013). Some studies have used precipitation data as an infiltration input signal (Rochet et al., 1994; Alfonsi, 1997; Zêzere et al., 2005; Meric et al., 2006; Zizioli et al., 2013). These approaches can lead to significant errors in estimates of infiltration and tend to under-estimate or over-estimate the destabilisation triggered by rainfall. In addition, in these studies, the methods and the recharge area parameters used to determine the recharge are rarely detailed and no turnkey method has so far been proposed to estimate simply and accurately the recharge.

The purpose of this study is to develop an efficient method in order to take into consideration the recharge in the studies of landslides with limited meteorological dataset. The objective of the method is to improve the reliability in calculation for the widest possible audience, by balancing the technical complexity and the accuracy. Indeed, landslide studies involve a wide range of specialities (sub-surface geophysics, structural geology, modelling, geotechnics, and geomechanics), for which scientists do not necessarily have the required hydrology training, but are nevertheless capable of following a simplified and robust method to compute the recharge.

To demonstrate that an accurate estimation of the recharge improves the characterization of the groundwater conditions which trigger the motion of deep-seated landslides, a simple linear correlation between recharge and displacement signals is carried out. The aim of the demonstration is to prove that recharge is a more relevant parameter than precipitation for accounting for the motion of deep-seated landslides, and is performed with no intention to model or to quantify the displacement.

2 Strategy and methods

2.1 Recharge computation strategy

The computation of the recharge has been simplified and detailed to increase its utility for the widest possible audience, without losing the accuracy required for its intended purpose (the prediction of slope displacement). The concept of requisite simplicity (Stirzaker et al., 2010) has been central to the design of an efficient method, balancing technical accuracy with utility for non-hydrologist users. It is thought that the method developed in this study is suitable for a typical scenario concerning both the availability of data for the site and the technical background of the user.

With respect to this aim, only the soil available water capacity (SAWC), the runoff coefficient, the vegetation coefficient and the evapotranspiration have been taken into account over the recharge area (averaged estimation for the whole recharge area). Evapotranspiration is the major factor influencing the recharge signal. Surface runoff is also a significant process to determine in order to accurately estimate the recharge. This is particularly true in mountainous areas or in areas prone to intense storms. Additional parameters such as the exposure to solar radiation or the influence of the unsaturated zone and discrete calculation could be taken into account, but at the expense of a greater complexity, with no guarantee of significantly improving the accuracy.

Typically, the deeper the aquifer, the slower the recharge and the more smoothed the recharge signal. However, a landslide is not a homogeneous medium. A part of the groundwater flows is slow and occur over several months, while another part is rapid and occur over a few days (Mudry and Etievant, 2007). Both slow and rapid flows play a role in landslide destabilization. A monthly resolution is therefore too long to take the groundwater response into account in the analysis. For a deep-seated landslide triggered by a deep water-saturated zone, the impact of a multi-day cumulative rainfall is far more significant than rainfall duration or intensity (Guzzetti et al., 2008). The hourly rainfall input signal is smoothed through hydrogeologic processes, depending on the hydrosystem inertia and connectivity. For these reasons, this study is based

HESSD

11, 6343–6403, 2014

Rainfall-triggered deep-seated landslides

A. Vallet et al.

[Title Page](#)

[Abstract](#)

[Introduction](#)

[Conclusions](#)

[References](#)

[Tables](#)

[Figures](#)

[⏪](#)

[⏩](#)

[◀](#)

[▶](#)

[Back](#)

[Close](#)

[Full Screen / Esc](#)

[Printer-friendly Version](#)

[Interactive Discussion](#)



on a daily time-step. The availability of the environmental data on a daily resolution determines which weather stations should be selected to supply the input data.

2.2 Method workflow

The recharge method workflow (Fig. 1) includes three steps. The first step consists of a regional calibration of reference vegetation evapotranspiration (ET_0) and solar radiation (R_S) reduced-set methods, with respect to the standard evapotranspiration method and direct measurements using reference weather stations recording all required parameters (detailed in Sect. 2.3). Calibrated methods then allow to estimate evapotranspiration at the landslide site equipped with a weather station measuring only temperature. The second step consists in estimating the vegetation coefficient, the SAWC, and the runoff coefficient across the recharge area using a GIS composite method (detailed in Sect. 2.4). The third step uses a soil–water balance to estimate the recharge with calibrated ET_0 and R_S reduced-set methods, and the estimation of the recharge area parameters (detailed in Sect. 2.5). Besides, a sensitivity analysis is performed in order to refine the SAWC and runoff coefficient estimations.

2.3 Methods calibration – Step 1

The regional method calibration is performed using the records of nearby weather stations (Fig. 1 – Step 1). These stations record the necessary meteorological parameters and will be referred to as reference weather stations. Calibrations of R_S and ET_0 reduced-set methods are performed for each reference weather station (local scale). The adjustment coefficients of the stations, deduced from the local calibration, are then averaged in order to define a regional calibration for sites where more than one reference station can be used. The elevation and the latitude of the reference weather stations should be within the range of the studied landslide site elevation and latitude. For sites with a sparse weather station network, one reference station can be sufficient

HESSD

11, 6343–6403, 2014

Rainfall-triggered deep-seated landslides

A. Vallet et al.

[Title Page](#)

[Abstract](#)

[Introduction](#)

[Conclusions](#)

[References](#)

[Tables](#)

[Figures](#)

[⏪](#)

[⏩](#)

[⏴](#)

[⏵](#)

[Back](#)

[Close](#)

[Full Screen / Esc](#)

[Printer-friendly Version](#)

[Interactive Discussion](#)



for the calibration, provided this station has the same weather conditions as those of the studied site.

The performance assessment and ranking of each of the regionally calibrated methods is based on the comparison between observed measurements and calibrated estimates. Performance indicators are the coefficient of determination (R^2), the slope and the intercept from linear regression (independent variable: estimated parameter; dependant variable: observed parameter), and the relative error RE (root mean square error, or RMSE, divided by the observed dataset mean).

2.3.1 Solar radiation methods

Bristow and Campbell (1984) and Hargreaves and Samani (1985) proposed each a reduced-set method to compute solar radiation (R_S) based on temperature (Eqs. A1 and A2 in Appendix A). Castellvi (2001) demonstrated that both methods show good results for daily frequencies. Almorox (2011) compared the performance of a more extensive list of temperature-based R_S methods which might be more suitable to local conditions at other landslide sites. In this study, the calibration of the R_S reduced-set method was performed using the following modified equations of which a constant is added to take into account eventuality of a R_S estimation shift from the original method:

Bristow–Campbell modified equation ($BC_{\text{mod}}R_S$):

$$BC_{\text{mod}}R_S = A_{BC}R_a \left[1 - \exp \left(-B_{BC}(\alpha\Delta T)^{C_{BC}} \right) \right] D_{BC} \quad (1)$$

Hargreaves–Samani modified equation ($HS_{\text{mod}}R_S$):

$$HS_{\text{mod}}R_S = A_{HS}R_a(\alpha\Delta T)^{B_{HS}} + C_{HS} \quad (2)$$

where A_{BC} , B_{BC} , C_{BC} , D_{BC} are the Bristow–Campbell regional calibration coefficients, A_{HS} , B_{HS} , C_{HS} are the Hargreaves–Samani regional calibration coefficients, α is the cloud cover adjustment factor.

The Bristow–Campbell coefficients have to be evaluated. The Hargreaves–Samani method coefficients have default values. However, Trajkovic (2007) showed that the regional calibration of the Hargreaves–Samani method (combining ET_0 and R_S methods) is significantly improved by coefficient adjustments rather than by linear regression.

Therefore, all the $HS_{mod}R_S$ coefficients are adjusted.

A cloud cover adjustment factor α is furthermore applied to ΔT since, for cloudy conditions, ΔT can produce an estimate larger than the incoming solar radiation (Bristow and Campbell, 1984). The α coefficient is applied for the two first rain event days since, for a rain period longer than two days, the temperature and R_S get equilibrated. If ΔT on the day before a rain event (ΔT_{j-1}) is less than ΔT_{j-2} by more than 2°C , the coefficient α is also applied assuming that cloud cover was already significantly present. For the remaining days, α is not applied ($\alpha = 1$). The 2°C threshold and the 2 days period are based on Bristow and Campbell (1984). In this study, the cloud cover adjustment factor α is calibrated according to site conditions. This approach is based on the principle that if this adjustment is not relevant, a calibrated α coefficient would be equal to 1 (no effect).

Adjustment of coefficients (including α) for the R_S regional calibration is non-linear. To adjust the calibration coefficients, a grid search iterative algorithm is used to maximise the value of R_S performance (Eq. 3).

$$R_S \text{ performance} = \frac{\sum_{i=1}^m (R_m^2 - RE_m)}{m} \quad (3)$$

where m is the number of weather stations used for the calibration, R^2 is the coefficient of determination and RE is the relative error, both R^2 and RE being computed between measured and estimated values at each weather station.

Rainfall-triggered deep-seated landslides

A. Vallet et al.

Title Page

Abstract

Introduction

Conclusions

References

Tables

Figures

⏪

⏩

◀

▶

Back

Close

Full Screen / Esc

Printer-friendly Version

Interactive Discussion



2.3.2 Evapotranspiration methods

The reference vegetation evapotranspiration (ET_0) is the evapotranspiration from a reference grass surface and is used as a standard from which specific vegetation evapotranspiration is deduced. The Penman–Monteith method has been extensively evaluated worldwide and is considered as the most widely accepted method for ET_0 estimation (Jensen et al., 1990). Following this work, Allen et al. (1998) in the paper FAO-56 (Food and Agriculture Organization of the United Nations) developed a modified form of the Penman–Monteith method (FAO-56 PM ET_0), which is adopted by the scientific community as a global standard method to estimate ET_0 worldwide.

Several reference vegetation evapotranspiration (ET_0) methods using a reduced dataset in comparison to FAO-56 PM ET_0 , have been developed worldwide. Only a few methods are commonly used. This is the case with the five ET_0 methods selected for this study, which have shown good performance when using daily to weekly frequencies (Trajkovic, 2005; Yoder et al., 2005; Alexandris et al., 2008; Shahidian et al., 2012; Tabari et al., 2013). The five ET_0 methods include one temperature-based method, that is the Hargreaves–Samani method (1985), four solar radiation/temperature-based methods, the methods of Makkink (1957), Turc (1961), and Priestley and Taylor (1972), and the Penman–Monteith reduced-set method (Allen et al., 1998) (Eqs. A4–A10 in Appendix A). The estimation of solar radiation with a R_S temperature-based method allows to compute the evapotranspiration with the five above ET_0 methods based only with temperature. The reference vegetation evapotranspiration (ET_0) corresponds to the maximum possible water loss by evaporation and transpiration from an actively growing grass with an extensive and uniform surface (Allen et al., 1998). The Priestley–Taylor and Penman–Monteith ET_0 reduced-set methods use net solar radiation (R_n) instead of R_S , which can be deduced from R_S with the Penman–Monteith reduced-set method assumptions (Allen et al., 1998). The foregoing ET_0 methods were developed for irrigation scheduling, for which the scope of application involves positive temperatures (plant water supply during the spring-summer growing period). However, in

HESSD

11, 6343–6403, 2014

Rainfall-triggered
deep-seated
landslides

A. Vallet et al.

Title Page

Abstract

Introduction

Conclusions

References

Tables

Figures

⏪

⏩

◀

▶

Back

Close

Full Screen / Esc

Printer-friendly Version

Interactive Discussion



mountainous sites, winter temperatures are often below 0°C, and ET_0 empirical methods can compute negative ET_0 values. Negative ET_0 computed values do not have any physical meaning and are therefore set to zero.

Previously cited ET_0 methods were developed for specific weather conditions. FAO-56 PM calculated data at reference weather stations are used as standards to calibrate the ET_0 reduced-set methods, in order to take into account the landslide site weather conditions. A linear regression is performed for each of the reduced-set evapotranspiration methods and for each weather station (Eq. 4). The slope a and the intercept b of the best-fit regression line obtained for each reference weather station are used as local calibration coefficients. Regional calibration coefficients are calculated by averaging the local coefficients of each reference weather station.

$$ET_{0\text{FAO-56 PM}} = aET_{0\text{method}} + b \quad (4)$$

where $ET_{0\text{FAO-56 PM}}$ is the reference vegetation evapotranspiration and $ET_{0\text{method}}$ is obtained by any of the five reduced-set methods tested in this study. The linear regression method has been widely used to calibrate ET_0 reduced-set methods (Allen et al., 1994; Trajkovic, 2005; Shahidian et al., 2012).

Reduced-set ET_0 methods do not take into account the wind speed variations. By removing saturated air from the boundary layer, wind increases evapotranspiration (Shahidian et al., 2012). Several studies show the influence of the wind speed on reduced-set ET_0 method performance and therefore on calibration (Itenfisu et al., 2003; Trajkovic, 2005; Trajkovic and Stojnic, 2007). For this study, the days with wind speed above the 95th percentile of the dataset (extreme values) were disregarded for the calibration.

The combination of calibrated ET_0 and R_S methods allows the estimation of ET_0 based only on temperature. The specific vegetation evapotranspiration (ET_c) is calculated by applying a vegetation coefficient (K_c) to ET_0 (i.e. $ET_c = ET_0 \times K_c$).

HESSD

11, 6343–6403, 2014

Rainfall-triggered deep-seated landslides

A. Vallet et al.

Title Page

Abstract

Introduction

Conclusions

References

Tables

Figures

⏪

⏩

◀

▶

Back

Close

Full Screen / Esc

Printer-friendly Version

Interactive Discussion



2.4 Recharge area: composite GIS – Step 2

No attempt of discrete calculation of recharge over the recharge area is undertaken in this study. The recharge area parameters (soil available water capacity SAWC, runoff coefficient, vegetation coefficient K_c) were assumed to be spatially uniform and constant over time (except for K_c which varies in time). However, the spatial heterogeneity of the recharge area was taken into account in order to estimate an average value for each parameter over the recharge area by performing a GIS composite method (Fig. 1 – Step 2). For one given parameter, the recharge area was divided into sub-areas, each being characterised by a constant value estimated according to field measurements, literature values or calculation. For each parameter, the matching sub-area is estimated by combining the different land use sub-areas which have an influence on the target parameter (for example vegetation + geology substratum). Sub-areas can be continuous or discontinuous, and their number and their geometry can differ according to land use spatial distribution. The parameters are subsequently estimated at the scale of the recharge area according to the sub-area surface (equation in Fig. 1 – Step 2). A wide range of input data (digital elevation model (DEM), aerial photographs, geological maps, field investigations and auger holes) were analysed and combined to estimate the three recharge area parameters required for recharge computation.

2.4.1 Vegetation coefficient (K_c)

The K_c coefficient gather together four primary characteristics that distinguish the vegetation from the reference grass: vegetation height, albedo, canopy resistance and evaporation from soil (Allen et al., 1998). As a consequence, the sub-areas were defined according to vegetation cover deduced from aerial photographs, with the main vegetation species described through field observations. Because the K_c coefficient is dependent on the vegetation development stages, it varies from a minimum during winter to a maximum during summer. For each sub-area, minimum and maximum K_c values were estimated from the literature and assigned respectively to 4 February (middle

HESSD

11, 6343–6403, 2014

Rainfall-triggered deep-seated landslides

A. Vallet et al.

Title Page

Abstract

Introduction

Conclusions

References

Tables

Figures



Back

Close

Full Screen / Esc

Printer-friendly Version

Interactive Discussion



of winter) and 6 August (middle of summer) of each year. A daily linear interpolation was performed for K_c between these two dates (Verstraeten et al., 2005).

2.4.2 Soil available water capacity (SAWC)

SAWC is mainly affected by soil texture and thickness, which primarily depends on geological substratum and vegetation cover. SAWC is also dependent on the root zone extent and the permanent wilting point, both variables according to vegetation type. Sub-areas were defined according to vegetation cover (deduced from aerial photographs) and according to geological substratum (deduced from geological maps). For each sub-area type, one auger hole was drilled at a representative location. SAWC is deduced from soil properties (type of horizon, texture and bulk density) and depth extent from auger hole cores, using a pedotransfer function (Jamagne et al., 1977; Bruand et al., 2004). SAWC values of auger holes are then assigned to the sub-area. The SAWC varies over time since water demand depends on the plant growing season. The SAWC dependency to vegetation species is taken into account through the K_c coefficient.

2.4.3 Runoff coefficient

Several rainfall–runoff models (Jakeman et al., 1991; Tan and O’Connor, 1996; Chiew et al., 2002; Brocca et al., 2011) have been designed for the purpose of hydrology, i.e. to characterise catchment outlet. They are not tailored for recharge estimation. Rainfall–runoff models require temporal flow calibration at the catchment outlet. In this study, there is no such outlet flow data, as most of the recharge area discharges into an alluvial aquifer at the landslide foot. As such, rainfall–runoff model calibration is not possible and this technique cannot be employed to estimate the recharge. The soil conservation service curve-number runoff method (SCS) designed for storm rainfall events rather than daily continuous estimation is also not suitable.

Rainfall-triggered deep-seated landslides

A. Vallet et al.

[Title Page](#)

[Abstract](#)

[Introduction](#)

[Conclusions](#)

[References](#)

[Tables](#)

[Figures](#)

[⏪](#)

[⏩](#)

[◀](#)

[▶](#)

[Back](#)

[Close](#)

[Full Screen / Esc](#)

[Printer-friendly Version](#)

[Interactive Discussion](#)



The runoff estimation method applied in this study is similar to the well-known and commonly used “runoff rational method”. The runoff coefficient depends mainly on the slope gradient and the vegetation cover. Sub-areas are defined according to vegetation cover deduced from aerial photographs. For each sub-area, an average slope gradient value is assigned, utilising DEM slope gradient analysis. For each sub-area, runoff coefficients are deduced from vegetation cover and slope gradient magnitude based on the Sautier chart (Musy and Higy, 2011). This chart was developed for Switzerland where environmental conditions are similar to the French Alps.

2.4.4 Infiltration structure

An additional sub-area type is defined to take into account preferential infiltration structures such as sinkholes, cracks, reverse slope areas, bare ground and any topographical depressions which can collect runoff. For such sub-areas, SAWC and runoff coefficient are very low and are considered to be null in the calculation at the scale of the recharge area. The consequence of preferential infiltration structures is a global decrease of SAWC and runoff coefficient values at the scale of recharge area. Infiltration structures are defined through inspection of aerial photographs (lineaments), geological mapping and field observations.

2.5 Soil–water balance: recharge computation – Step 3

Recharge is estimated according to the following soil–water balance with the ET_0 computed with the combination of R_S and ET_0 reduced-set calibrated methods and the SAWC, the vegetation coefficient and the runoff coefficient deduced from the GIS method (Fig. 1 – Step 3).

The precipitation (P) is the amount of liquid (rain) or solid (snow) water which falls on the recharge area. However, in the remaining part of the paper, the precipitation will be considered to be the same as the sum of snow melt and rainfall. A part of this water amount is intercepted by the vegetative canopy (interception) (Fig. 2). The remainder

Title Page

Abstract

Introduction

Conclusions

References

Tables

Figures

⏪

⏩

◀

▶

Back

Close

Full Screen / Esc

Printer-friendly Version

Interactive Discussion



of precipitation reaches the ground surface and forms: (i) the runoff (R_f), which is the water joining the surface drainage network; and (ii) the infiltration (I) into the soil layer which supplies the SAWC (also called soil available moisture capacity). The SAWC is the maximum soil water content available for evapotranspiration. The remaining part of the precipitation which has not been taken off by evapotranspiration and runoff and which has not been stored in the SAWC is called the recharge (R). It corresponds to deep percolation and it is the component of the rainfall which recharges the saturated zone (Fig. 2).

SAWC refers to the difference between a maximum water content above which all free water is drained through gravity (field capacity) and a minimum moisture content below which plant roots cannot extract anymore water (permanent wilting point). The difference between the maximum of SAWC and the actual SAWC is called the SAWC deficit ($SAWC_{max} - SAWC_{j-1}$ in Fig. 2b).

The canopy reservoir capacity was not evaluated in this study and therefore water evaporated by the interception process is taken off the SAWC reservoir (Fig. 2b). Evapotranspiration is the total evaporative loss from the surface, i.e. evaporation from soil and plants (interception), and transpiration from plants. Interception is the part of precipitation which is caught by leaves and branches, and which is subsequently evaporated.

The specific vegetation evapotranspiration (ET_c), deduced from ET_0 method and vegetation coefficient, is the water evapotranspired without any restrictions other than the atmospheric demand (assuming unlimited soil water availability). However, field conditions do not always fulfil these requirements, particularly during low rainfall periods, when water supplies are inadequate to support vegetation uptakes. Actual evapotranspiration (ET_a) corresponds to the actual amount of evapotranspired water.

Runoff takes place when the intensity of a precipitation event exceeds the soil infiltration capacity. The use of a daily measurement frequency for precipitation does not allow an accurate estimation of rainfall intensity (hourly rainfall resolution is not available). Instead, a runoff coefficient (R_{coeff}) is applied only for days when precipitation is

Rainfall-triggered deep-seated landslides

A. Vallet et al.

Title Page

Abstract

Introduction

Conclusions

References

Tables

Figures

◀

▶

◀

▶

Back

Close

Full Screen / Esc

Printer-friendly Version

Interactive Discussion



greater than the average. Such days are considered as high intensity rainfall days. The runoff coefficient is applied only to excess precipitation, after the demands of evapotranspiration and SAWC are met (i.e., when SAWC is fulfilled) (Fig. 2b).

The soil–water balance workflow used to estimate the recharge at a daily frequency is detailed in Fig. 2b. Each term (P , R_f , I , ET_a , ET_c , SAWC and R) is expressed in water amount (millimetres), except for R_{coeff} which is expressed in %.

2.6 Sensitivity analysis of the recharge area parameters

In the landslide recharge area, infiltration can be assumed to be spatially heterogeneous. Indeed, in fractured rock hydrogeology, the groundwater flow is mainly driven by an anisotropic fracture network. The proportion of infiltrated water which flows toward the landslide aquifer can be significantly different between two zones of the recharge area. Nevertheless, the GIS composite method considers that any part of the recharge area has the same weigh relatively to the infiltrated water which flows toward the landslide aquifer (i.e., homogeneous infiltration). This homogeneous assumption can lead to a bias estimation of the recharge area parameters.

On the other hand, numerous uncertainties remain about the recharge area delimitation, the SAWC estimation and the canopy reservoir influence. These uncertainties can also lead to biases in the recharge area parameters estimation. First, the delimitation of the recharge area only approximates the boundary of the actual recharge area. Secondly, the SAWC is deduced from soil properties and depth extent. However, variations in the root zone of different vegetation types have not been evaluated. Finally, for this study, the canopy reservoir is not evaluated in the soil–water balance which considers, by default, that the SAWC reservoir combines the water storage of both soil and canopy.

A sensitivity analysis is performed to evaluate the overestimation or underestimation of recharge area parameters. Infiltration structures are used as a fitting factor (varying from 0 to 100 % of the recharge area) to adjust the recharge area parameter estimation based on a heterogeneous assumption (identical land use properties but different

Rainfall-triggered deep-seated landslides

A. Vallet et al.

[Title Page](#)

[Abstract](#)

[Introduction](#)

[Conclusions](#)

[References](#)

[Tables](#)

[Figures](#)

[⏪](#)

[⏩](#)

[⏴](#)

[⏵](#)

[Back](#)

[Close](#)

[Full Screen / Esc](#)

[Printer-friendly Version](#)

[Interactive Discussion](#)



infiltration contribution weight to the landslide aquifer). A variation of the infiltration structure percentage corresponds to a variation of the infiltration structures contribution weight to the recharge of the landslide aquifer. As a consequence, a percentage variation of the infiltration structure does not affect the sub-area surfaces, which remain the same, but only their weights. In summary, with the assumption of an homogeneous infiltration, the recharge area parameters are defined from sub-area surfaces, while in the case of the heterogeneous infiltration assumption, the recharge area parameters are defined according to the sub-area infiltration contribution proportion (weighting) to the landslide aquifer.

The sensitivity analysis is based on rainfall–displacement correlation performance. The displacement velocity of the landslide triggered by rainfall depends on the groundwater saturation state and is therefore representative of the hydrodynamic variations. For this reason, rainfall–displacement correlation performance informs whether the recharge area parameters are suitable to characterise the water infiltration flowing toward the landslide aquifer.

The sensitivity analysis allows to determine the recharge area parameters which maximize the rainfall/displacement correlation performance. The SAWC estimation deduced from the sensitivity analysis will take into account the contribution of canopy storage and vegetation cover.

2.6.1 Saturation state approximation of the landslide triggering aquifer

The groundwater hydrodynamic processes due to aquifer drainage are non-linear. An ancient rainfall event displays less impact (though not null) than the most recent one on the aquifer saturation state (Canuti et al., 1985; Crozier, 1986). As a consequence, in this study, the aquifer saturation state is approximated by an antecedent cumulative sum amount of precipitation/recharge weighted by a decreasing factor (α) (Eq. 5). The antecedent cumulative sum corresponds to the total amount of rainfall that occurred over a defined period prior to a date. In Eq. (5), for α equalling zero, the decreasing

Rainfall-triggered deep-seated landslides

A. Vallet et al.

[Title Page](#)

[Abstract](#)

[Introduction](#)

[Conclusions](#)

[References](#)

[Tables](#)

[Figures](#)



[Back](#)

[Close](#)

[Full Screen / Esc](#)

[Printer-friendly Version](#)

[Interactive Discussion](#)



sum matches a classic arithmetic sum of rainfall.

$$\text{Decreasing sum} = \sum_{i=1}^n \frac{W_{i+\beta}}{1 + \alpha(i-1)} \quad (5)$$

where: n = cumulative period (day), $i = i$ th day, W_i = water input: precipitation or recharge at the i th day (mm), α = weighting factor, β = shift factor (day).

5 2.6.2 Rainfall–displacement correlation

Linear regressions between cumulative precipitation and displacement and/or between cumulative recharge and displacement are performed for each decreasing sum type, with n ranging from 1 to 250 days (1 day increment), α ranging from 0 to 0.5 (increment 0.001) and β ranging from 1 to 10 days (increment 1). The coefficient of determination (R^2) is used to assess the performance of rainfall–displacement correlation. An iterative grid search algorithm is used to find the best solution based on R^2 .

Between two correlation performance solutions, a small improvement of the R^2 value can be the result of adding an extra long computation period to which very low weighting factors are associated. The increase of the period computation to which low weights are applied acts as a smoothing function. The correlation improvement is explained by the randomness/noise smoothing of input signal rather than by a physical process. A R^2 tolerance of 0.001 for the best correlation performance is implemented. The correlation performance which ranges within the R^2 tolerance window and which has the lowest computation period is then selected as the best solution.

20 2.6.3 Significance of rainfall–displacement correlation

The significance is evaluated only for the characterization of the relationship between precipitation/recharge and displacement. The significance of R^2 for solar radiation and evapotranspiration calibration is not evaluated, because the purpose of the calibration

Rainfall-triggered deep-seated landslides

A. Vallet et al.

Title Page

Abstract

Introduction

Conclusions

References

Tables

Figures

⏪

⏩

◀

▶

Back

Close

Full Screen / Esc

Printer-friendly Version

Interactive Discussion



was only to tune adjustment coefficients and the significance of the relationship is not on purpose.

The bootstrap method, which is an inference statistical resampling method, is used to estimate the confidence interval (CI) of estimated parameters and to perform statistical hypothesis tests (Chernick, 1999). The bootstrap method uses resampling with replacement and preserves the pair-wise relationship. However, for dependent data (such as time series), the structure of the dataset has to be preserved during the resampling. The moving block bootstrap is a variant of the bootstrap method. It divides data into blocks for which the structure is kept, which makes it suitable for times series (Cordeiro and Neves, 2006). The moving block bootstrap method is performed with a 90 day block size (season) and 50 000 iterations for each run.

To estimate the significance of the linear regression, the lower bound of the confidence interval (LBCI) of R^2 is used at the level of confidence of 95 %. An LBCI value greater than 0 means that the relationship is significant.

Particular to statistical hypothesis tests is the definition of the tested null hypothesis which is often a default position opposite to the aim of the test, i.e. “there is no relationship between two quantities”. The null hypothesis is assumed to be true until it is rejected by statistical evidence in favour of the alternative hypothesis (that is the contrary).

To estimate whether the recharge/displacement correlation R^2 is significantly better than the precipitation/displacement correlation R^2 value, the Null Hypothesis 1 (NH1) was tested. The NH1 states that the recharge/displacement correlation R^2 value is not significantly greater than the R^2 value obtained with precipitation. In other words, the NH1 statistic test is the difference between the recharge R^2 value and the precipitation R^2 value, expected to be 0 if no differences.

To estimate whether the best rainfall/displacement correlation R^2 value computed from the sensitivity analysis is significantly better than the other R^2 values obtained, the Null Hypothesis 2 (NH2) was tested. The NH2 states that the best R^2 value is not significantly greater than the ones obtained with all the remaining combinations. In

Rainfall-triggered deep-seated landslides

A. Vallet et al.

Title Page

Abstract

Introduction

Conclusions

References

Tables

Figures



Back

Close

Full Screen / Esc

Printer-friendly Version

Interactive Discussion



other words, the NH2 statistic test is the difference between the best R^2 value and the R^2 values obtained with the remaining combinations, expected to be 0 if no differences.

For both null hypotheses NH1 and NH2, the decision to reject the null hypothesis is made by determining how much of the bootstrap distribution (among 50 000 iterations) falls below zero by using the lower bound of the confidence interval (LBCI) at the level of confidence of 95 %. An LBCI value greater than 0 allow to reject the null hypotheses.

3 Application to the S echilienne landslide

Several studies on the S echilienne landslide concerning the rainfall trigger use precipitation or indirect infiltration estimates (Rochet et al., 1994; Alfonsi, 1997; Meric et al., 2006; Helmstetter and Garambois, 2010). Similarly, the warning system of S echilienne is partly based on precipitation. S echilienne landslide investigations and the warning system could be significantly improved by evaluating recharge instead of precipitation.

3.1 Context

The S echilienne landslide is located 25 km south-east of Grenoble, (France), on the right bank of the Romanche River, on the southern slope of the Mont-Sec Massif. The site is located in the external part of the French Alps, in the Belledonne crystalline range. The geological nature of the area is composed of vertical N–S foliated micaschists unconformably covered by Carboniferous to Liassic sedimentary deposits along the massif ridge line above the unstable zone (Fig. 3). Locally, Quaternary glacio-fluvial deposits overlie these formations. The landslide is delineated to the east by a major 20° N trending fault zone. Two major wrench faults, 140° N dextral and 20° N sinistral, compartmentalize the disturbed zone into blocks. The slope is cut by a dense network of two conjugate sub-vertical fracture sets, striking 140° N and 50–70° N (Vengeon, 1998). The latter divides the slope into numerous sub-vertical compartments.

HESSD

11, 6343–6403, 2014

Rainfall-triggered deep-seated landslides

A. Vallet et al.

[Title Page](#)

[Abstract](#)

[Introduction](#)

[Conclusions](#)

[References](#)

[Tables](#)

[Figures](#)

[⏪](#)

[⏩](#)

[⏴](#)

[⏵](#)

[Back](#)

[Close](#)

[Full Screen / Esc](#)

[Printer-friendly Version](#)

[Interactive Discussion](#)



3.2 Deformation mechanism and rainfall triggering

An originality of the Séchilienne landslide is the absence of a well defined basal sliding surface. The Séchilienne landslide deep-seated progressive deformation is controlled by the main discontinuities (faults/fractures). The slope is affected by a toppling movement of the 50–70° NE striking blocks toward the valley, coupled with the subsidence of the upper part of the slope near Mont-Sec. This mechanism has been described by Vengeon (1998) as an internal rupture mechanism. The landslide displacement velocity smoothes progressively toward the west and the slope foot, whereas it drops abruptly beyond the 20° N trending fault zone delimiting the eastern boundary.

The groundwater flow is mainly driven through a network of fractures with relatively high flow velocities (km day^{-1}). The moving zone, about 150 m deep (Le Roux et al., 2011), shows a higher hydraulic conductivity than the bedrock (Vengeon, 1998) and constitutes a perched aquifer (Guglielmi et al., 2002). The landslide displacement has caused a wide opening of the fractures. The groundwater flow mechanisms that are responsible for recharge in the disturbed zone are not agreed upon. Vengeon (1998) shows that the moving zone perched aquifer is recharged by water-level rise of the deep saturated zone whereas Guglielmi et al. (2002) showed that the main recharge originates from the top sedimentary perched aquifer. Increases in pore water pressure originate in the disturbed zone, leading to landslide displacement. As a result, the Séchilienne landslide shows a good correlation between antecedent cumulative precipitation and average displacements (Rochet et al., 1994; Alfonsi, 1997). Helmstetter and Garambois (2010) showed a weak but significant correlation between rainfall signals and rock fall micro-seismicity. Instability in the Séchilienne slope is mainly triggered by rainfall events.

3.3 Dataset

The selected weather stations satisfy two conditions: (i) they record all the required parameters to compute ET_0 with standard FAO-56 PM (wind speed, relative humidity,

HESSD

11, 6343–6403, 2014

Rainfall-triggered deep-seated landslides

A. Vallet et al.

Title Page

Abstract

Introduction

Conclusions

References

Tables

Figures



Back

Close

Full Screen / Esc

Printer-friendly Version

Interactive Discussion



temperature, solar radiation or relative sunshine duration, measured daily); and (ii) they are located less than 60 km from the site. Three stations, managed by MétéoFrance, fulfill these requirements: Grenoble-Saint-Geoirs, Saint-Jean-Saint-Nicolas and Saint-Michel-Maur (Table 1 and Fig. 3). The Saint-Michel-Maur weather station does not measure R_S . However R_S can be calculated with the Angström formula (Eq. A3 in Appendix A) using sunshine duration data recorded at the station (FAO-56 guidelines, Allen et al., 1998). The Angström formula empirical default coefficients were tuned with the two others weather stations ($a_S = 0.232$ and $b_S = 0.574$). The recharge computation was based on the rainfall recorded at the weather station located at Mont-Sec, a few hundred meters above the top of the disturbed zone (Table 1 and Fig. 3). This station is equipped with rain and snow gauges.

Although this study aims at estimating recharge using only temperature and precipitation dataset, temperature measurements at the Mont-Sec station are considered unreliable because of temperature sensor non-standard setting and numerous missing data. In order to estimate a representative daily temperature dataset for the site, the two nearest weather stations measuring temperature, named Luitel and La Mure, were used (Table 1 and Fig. 3). The estimation of the Mont-Sec temperature is detailed in Appendix B.

Aerial photographs of 0.5 m resolution and a digital elevation model (DEM) of 25 m resolution were provided by the “Institut National de l’Information Géographique et Forestière” (IGN). Geological maps from the French Geological Survey (BRGM) were used to determine the geology and faults within the recharge area.

The Séchillienne landslide is permanently monitored by several displacement stations using a variety of techniques (extensometers, radar, infra-red, inclinometers, GPS). This dense network has been implemented by the CEREMA Lyon (Duranthon et al., 2003). For the present study, one infra-red (named 1101) and three extensometer (named A16, A13 and G5) stations have been used. 1101, A16 and A13 are located on the surface of the most active unstable zone which is also the most reactive zone with respect to rainfall events (Fig. 3). The A16 extensometer was used for

HESSD

11, 6343–6403, 2014

Rainfall-triggered deep-seated landslides

A. Vallet et al.

Title Page

Abstract

Introduction

Conclusions

References

Tables

Figures



Back

Close

Full Screen / Esc

Printer-friendly Version

Interactive Discussion



the sensitivity analysis whereas the three other stations were only used for rainfall–displacement correlation purposes. The sensitivity analysis is performed on the period from 1 May 1994 to 1 January 2012, period during which both A16 extensometer and recharge datasets are available. In order to compare the rainfall–displacement correlation performance of the four selected stations, the correlation is performed on the period from 1 January 2001 to 1 January 2012, period during which the fours extensometers and recharge datasets are available.

3.4 Displacement data

The long-term displacement monitoring of the most active zone of the Séchilienne landslide shows that displacement rates and amplitudes have significantly increased over time as illustrated with the records of the extensometer A16 (Fig. 6a). This increase is also observed for all the records even the G5 station located in a less active zone. The trend could be the result of a deterioration of near-surface rock mechanical properties or of a change of behaviour in groundwater hydrodynamics (Rutqvist and Stephansson, 2003). It means that for the same amount of rainfall, the displacement rate and the displacement amplitude are not the same over time. In terms of time series analysis, the displacement data series shows a trend on the variance amplitude as well as on the average. The observed trend is not dependent on rainfall, but finds its origin in the modification of landslide mechanical properties. In order to perform a pluri-annual comparison between the rainfall signal and the displacement signal, the trend of displacement data for the four stations has been removed (detrending).

The trend was defined by fitting a fourth-order polynomial to the recorded displacement. Removal of the trend was performed with the multiplicative method (i.e., time series is divided by the trend) which results in a unitless time series with both variance and mean trend removed. The trend characterization is a statistical process which is enhanced by increasing the amount of data used in the process. Using a larger framing interval allows to reduce edge effects, which can be particularly high for the upper bounds of the interval (exponential pattern). For this reason, the detrending was

Rainfall-triggered deep-seated landslides

A. Vallet et al.

[Title Page](#)

[Abstract](#)

[Introduction](#)

[Conclusions](#)

[References](#)

[Tables](#)

[Figures](#)

[⏪](#)

[⏩](#)

[◀](#)

[▶](#)

[Back](#)

[Close](#)

[Full Screen / Esc](#)

[Printer-friendly Version](#)

[Interactive Discussion](#)



performed on a larger interval than the one used for rainfall–displacement correlation. An example of trend removal by the multiplicative method is shown in Fig. 6 for the extensometer A16 record. A16 record trend is defined from 6 March 1994 to 30 June 2012 whereas detrending is performed from 1 May 1994 to 31 December 2011.

5 The detrended displacement data of the four displacement stations are then used for the correlation with precipitation and recharge.

4 Results and discussion

4.1 Calibration of methods

4.1.1 Solar radiation methods

10 Data used for calibration are from 8 July 2009 to 1 January 2012 at Grenoble-Saint-Geoirs (907 records) and from 1 January 2004 to 1 January 2012 for both Saint-Jean-Saint-Nicolas (2876 records) and Saint-Michel-Maur (2864 records) weather stations. The two calibrated methods show good results with respect to R_S measured at the weather stations (Table 2). The $BC_{\text{mod}}R_S$ method is selected as it shows a better performance ($R^2 = 0.864$; RE = 0.119) than the $HS_{\text{mod}}R_S$ method ($R^2 = 0.847$; RE = 0.123).
15 Equation (6) presents the calibrated BC R_S method with all the calibrated coefficients.

$$BC_{\text{mod}}R_S = 0.669R_a[1 - \exp(-0.010(\alpha\Delta T)^{2.053})] + 1.733 \quad (6)$$

The cloud cover adjustment factor α is either equal to 0.79 (calibrated) or to 1, according to the conditions mentioned in Sect. 2.5.1. All the equation terms are described in the respective references (Appendix A). The $BC_{\text{mod}}R_S$ calibrated method is used to
20 compute R_S input data of the five ET_0 reduced-set methods.

Rainfall-triggered deep-seated landslides

A. Vallet et al.

Title Page

Abstract

Introduction

Conclusions

References

Tables

Figures

⏪

⏩

◀

▶

Back

Close

Full Screen / Esc

Printer-friendly Version

Interactive Discussion



4.1.2 Evapotranspiration methods

The data period used for ET_0 method regional calibration was the same as the one for R_S calibration. However strong wind days were removed. Overall, all of the ET_0 methods tested show good results for regional calibration, and are all suitable for the S echilienne site (Table 3). PS ET_0 , Turc ET_0 and M ET_0 methods a and b coefficients show that the regional calibration is required (Table 3). Conversely, PM red ET_0 and HS ET_0 methods a and b coefficients show that these methods have reliable performance even without regional calibration for the S echilienne site.

Among the ET_0 methods tested, $PM_{red}ET_0$ method shows the best performance ($R^2 = 0.932$; $RE = 0.221$) and requires only a low regional adjustment. Therefore, the $PM_{red}ET_0$ method was selected to compute ET_0 for the S echilienne site ($ET_0^{S ech}$). Figure 4 displays the estimated $PM_{red}ET_0$ vs. the FAO-56 PM computation for each reference weather station. Equation (7) is the final calibrated $PM_{red}ET_0$ method with all the calibrated coefficients. The input R_n term is deduced from the calibrated $BC_{mod}R_S$ method.

$$ET_{0}^{S ech} = 0.994 \frac{0.408\Delta (R_n - 0) + \gamma \frac{900}{T_{avg} + 273} 1.5(e_s - e_a)}{\Delta + \gamma(1 + 0.34 \cdot 1.5)} + 0.013 \quad (7)$$

Although the HS ET_0 method does not produce a performance as good as the PM red ET_0 method, it is one of the simplest methods from the five methods tested. The HS ET_0 method constitutes a simpler alternative for ET_0 estimation on the S echilienne site. The HS ET_0 method shows an acceptable performance when used for rough ET_0 estimation without calibration. Equation (8) presents the combination of calibrated $BC_{mod}R_S$ and calibrated HS ET_0 methods with all the calibrated coefficients. All the equation terms are described in the respective equation references (Appendix A).

$$ET_0 = 0.920 \cdot 0.0135 \cdot 0.408(0.669R_a[1 - \exp(-0.010(\alpha\Delta T)^{2.053})] + 1.733)(T_{avg} + 17.8) + 0.130 \quad (8)$$

In the remaining part of this paper, the evapotranspiration component ET_c will be computed with the calibrated PM red ET_0 method (Eq. 7), of which the R_n term is deduced from the calibrated $BC_{mod}R_S$ method (Eq. 6) and K_c coefficients.

4.2 Recharge area parameters

The overall recharge area is delimited by taking into account: (i) the results of natural tracing combined with a tracer test which demonstrates that the highest summits of the massif contribute to the recharge area (Mudry and Etievant, 2007); (ii) the results of a $\delta^{18}O$ survey, which confirm that remote, high elevation areas (up to 3 km away) fall within the recharge area of the landslide (Guglielmi et al., 2002); and (iii) topographical and geological maps.

Sub-areas are expressed in percentages of the whole recharge area (Table 4 and Fig. 5). Two types of vegetation cover, pasture and forest, are delineated using aerial photographs, with proportions of 23 % and 53 %, respectively. Three main geology sub-areas, micaschist bedrock (15 %), sedimentary cover (20 %) and superficial formations (41 %), are defined through examination of the geological map and field investigations. Infiltration structures are centred on the major faults as identified on the geological map, the lineaments deduced from an analysis of the aerial photographs and the geomorphological features (sinkholes, cracks) for which a 50 m wide influence zone surrounding the identified objects is added, leading to a sub-area representing 24 % of the recharge area.

4.2.1 Vegetation coefficient (K_c)

The Séchillienne forest is mainly composed of beech (*Fagus sylvatica*) and conifer (*Picea excelsa*) trees, which can be associated occasionally with ash (*Fraxinus*) and sweet chestnut (*Castanea sativa*) trees. The proportion of beech and conifer was assumed to be identical for the Séchillienne forest (each 50 % of forest sub-area) and other species were ignored for K_c estimation. Vegetation coefficient (K_c) were set to

Rainfall-triggered deep-seated landslides

A. Vallet et al.

[Title Page](#)

[Abstract](#)

[Introduction](#)

[Conclusions](#)

[References](#)

[Tables](#)

[Figures](#)

[⏪](#)

[⏩](#)

[⏴](#)

[⏵](#)

[Back](#)

[Close](#)

[Full Screen / Esc](#)

[Printer-friendly Version](#)

[Interactive Discussion](#)



0.71 and 0.97 for conifer, and to 0.78 and 0.9 for beech trees (Verstraeten et al., 2005). Most of the pastures are anthropogenic and consist of grass ($K_c = 0.85$ to 1, Allen et al., 1998). Infiltration structure sub-areas are not taken into account in the K_c estimation, so the relative proportions of pasture and forest become 30 % and 70 %, respectively.

5 The contribution of each sub-area is estimated (Table 4, column “ K_c RA”), allowing the determination of the recharge area K_c values (0.777 to 0.955).

4.2.2 Soil available water capacity (SAWC)

The combination of geology and vegetation sub-areas results in six combined sub-areas for the recharge area (Table 4). SAWC values based on soil auger investigations are assigned to each sub-area. The contribution of each sub-area to the average recharge area estimation is derived from the GIS composite method. The average estimation of SAWC at the recharge area scale is 106 ± 10 mm (rounded to 105 mm).

4.2.3 Runoff coefficient

15 An average slope gradient is computed from slope gradient analysis and is assigned to each vegetation sub-area. Pasture and forest sub-areas show an average slope gradient of 14° and of 20.6° respectively. Runoff coefficients of 22 % for pasture and 15 % for forest are deduced from the Sautier chart. A 12.8 % runoff coefficient is then estimated at the recharge area scale, according to the respective proportions of sub-areas in the recharge area (Table 4).

4.3 Sensitivity analysis

20 The data period for rainfall–displacement correlation is from 1 May 1994 to 1 January 2012 (6454 records). This is a common data interval for A16 extensometer and Mont-Sec weather station records. Because the recharge is computed since 9 September 1992 onwards, there are no edge effects due to SAWC initial conditions (sufficient time to equilibrate in the soil–water balance process).

Title Page

Abstract

Introduction

Conclusions

References

Tables

Figures

⏪

⏩

◀

▶

Back

Close

Full Screen / Esc

Printer-friendly Version

Interactive Discussion



Rainfall-triggered deep-seated landslides

A. Vallet et al.

Title Page

Abstract

Introduction

Conclusions

References

Tables

Figures

⏪

⏩

◀

▶

Back

Close

Full Screen / Esc

Printer-friendly Version

Interactive Discussion



Although the sensitivity analysis is based on infiltration structure percentage, the results of the sensitivity analysis are described according to the corresponding estimated SAWC values. SWAC parameter is more informative than an infiltration structure percentage. Sensitivity analysis is performed for SAWC ranging from 0 (100% of infiltration structures corresponding to precipitation) to 145 mm of SAWC (0% infiltration structures +10 mm of SAWC uncertainties measurement) with an increment of 10 mm. The coupled surface runoff coefficient ranges from 0 to 16.3% (in increments of about 1%). For each combination, recharge is computed according to the soil–water balance (Fig. 1 – Step 3 and Fig. 2) with: (i) the temperature estimated for the recharge area (Appendix B), (ii) the precipitation recorded at Mont-Sec weather station, and (iii) the properties of the recharge area.

All the best computations have a one-day lag, with periods ranging from 56 to 104 days (Table 5). The best R^2 obtained from recharge is obtained with both the homogeneous infiltration assumption (SAWC = 105 mm, $R^2 = 0.618$) and the heterogeneous infiltration assumption for SAWC from 85 ($R^2 = 0.618$) to 115 mm ($R^2 = 0.617$). For all the recharge combinations tested, the LBCI values from bootstrap testing of NH1 are greater than 0, allowing to reject the null hypothesis NH1 (Fig. 7c). In other words, it shows that the R^2 obtained with recharge is always significantly higher than the one computed with precipitation ($R^2 = 0.311$) even for a SAWC of 5 mm ($R^2 = 0.426$) (Table 5).

One of the best correlation performances is obtained with the homogeneity assumption. This reveals that the delimitation of the recharge area reflects properly the Séchillenne landslide groundwater contributing recharge area. For the heterogeneous infiltration scenarios having SAWC values above 55 mm, the LBCI values from bootstrap testing of NH1 from are lower than 0, not allowing to reject the null hypothesis NH2 (Table 5 and Fig. 7d). In other words, it shows that the R^2 obtained with the homogeneous assumption (SAWC = 105 mm) is not significantly higher than the ones from the heterogeneous assumption with SAWC above 55 mm. The best correlation from the sensitivity analysis can be influenced by local properties of the A16 extensometer

location and it is possible that infiltration structures could gather a large proportion of the flow (up to 61 % for SAWC = 55 mm) relative to their recharge surface area (24 %) (Table 5). If so, fractures can play an important role in the groundwater drainage from the massif towards the landslide aquifer.

Recharge-displacement correlations for SAWC values ranging from 75 (runoff = 9 %) to 115 mm (runoff = 13.9 %) show (i) a cumulative period computation (n) below 101 days, that is within the third quartile, (ii) an R^2 greater than 0.616, that is within the third quartile and (iii) LBCI values of NH2 greater than 0 (Table 5 and Fig. 7). This SAWC and runoff range seems to statistically reflect the recharge area properties of the landslide, and is recommended for further work on the Séchilienne landslide. For the remaining part of this paper, the homogeneous infiltration assumption (SAWC = 105 mm) will be preferred to the heterogeneous assumption because it is based on actual field observation data.

Figure 8 shows the best correlation results of cumulative precipitation and recharge (SAWC = 105 mm) together with A16 detrended displacement. The cumulative recharge signal reproduces well the displacement acceleration and deceleration phases, and especially the dry summers where displacement dropped dramatically (summers 1997, 1998, 2003, 2004 and 2009, Fig. 8b). On the contrary, the cumulative precipitation signal is more contrasted and more noisy, and does not manage to reproduce many peaks (width and intensity) of the detrended displacement signal (winters 1997, 2000, 2004, 2005 and 2010). In addition, the cumulative precipitation signal shows a weak correlation with displacement deceleration phases (summers 1998, 1999, 2000 2006, 2009 and 2010).

Because the displacements of deep-seated landslides are strongly correlated with pore water pressures, the weakness of the correlation performance ($R^2 < 0.7$) can be explained by the fact that all the displacement data are correlated, not only the displacement acceleration stages. Indeed, the displacement rate depends on rock properties and aquifer hydrodynamics, which behave differently according to either acceleration or deceleration stages.

Rainfall-triggered deep-seated landslides

A. Vallet et al.

[Title Page](#)

[Abstract](#)

[Introduction](#)

[Conclusions](#)

[References](#)

[Tables](#)

[Figures](#)



[Back](#)

[Close](#)

[Full Screen / Esc](#)

[Printer-friendly Version](#)

[Interactive Discussion](#)



4.4 Relevance of recharge signal for the Séchilienne landslide

The recharge is computed according to the homogeneous assumption (i.e. infiltration structures = 24 %, SAWC = 105 mm, and runoff coefficient = 12.8 %) and is compared with the precipitation signal (Fig. 9). The recharge signal differs significantly from the precipitation signal, especially during summer when ET_c is important. Indeed, the first rainfall events after a dry period do not reach the aquifer until the SAWC is exceeded.

In order to assess whether the recharge is a relevant parameter for the Séchilienne landslide, the correlation between rainfall and displacement was tested against four displacement stations (Fig. 3) on their common data interval (1 January 2001 to 1 January 2012). Stations 1101, A13 and A16 are representative of the most active zone (median displacement of 2.5, 1.75 and 2.98 mm day⁻¹, respectively), while G5 is located on a much less active zone (median displacement of 0.05 mm day⁻¹) (Table 6). All LBCI values from bootstrap testing of NH1 are greater than zero, allowing to reject the null hypothesis NH1. Rejection of NH1 shows that the R^2 obtained with recharge are significantly higher than the ones computed with precipitation for the four stations (Fig. 10). R^2 varies from 0.243 to 0.586 for recharge and from 0.0006 to 0.343 for precipitation, for G5 and A16 extensometer respectively (Table 6). However, the 2.5th and 97.5th percentile of NH1 bootstrap distribution and the observed value of NH1 test are rather constant for the four displacement stations, respectively about 0.145, 0.250 and 0.325 (Fig. 10). In other words, recharge is more significant than precipitation at the same level for the four stations whereas correlation with displacement is very variable. This may be explained by the fact that groundwater hydrodynamic probably triggers the entire Séchilienne landslide while the displacement velocity response depends on the damage level of the rock of the displacement station location. This interpretation is supported by the variability of the cumulative period, the shift factor, the weighting factor and the R^2 value especially between G5 and the three others stations (Table 6). Finally, concerning the A16 extensometer, R^2 is better on the short interval (0.343) than the one from the sensitivity analysis (0.311) for precipitation and inversely for the

HESSD

11, 6343–6403, 2014

Rainfall-triggered deep-seated landslides

A. Vallet et al.

Title Page

Abstract

Introduction

Conclusions

References

Tables

Figures



Back

Close

Full Screen / Esc

Printer-friendly Version

Interactive Discussion



recharge (0.586 instead of 0.618 for the sensitivity analysis). This could be the consequence of a degradation of near-surface rock mechanical properties of the Séchillienne landslide (as suggested by the displacement trend, Fig. 6) which makes the landslide more sensitive to precipitation events in the recent period.

5 4.5 Applicability to other landslides

Several studies have shown the relevance of recharge for coastal landslides (Maquaire, 2000; Bogaard et al., 2013), unstable embankment slope landslides (Cartier and Pouget, 1987; Delmas et al., 1987; Matichard and Pouget, 1988) and deep-seated earthflow landslides (Malet et al., 2003; Godt et al., 2006). In addition, destabilization of shallow landslides is known to be influenced by antecedent soil moisture and precipitation (Brocca et al., 2012; Garel et al., 2012; Ponziani et al., 2012). Recharge, which implicitly gathers together antecedent soil moisture and precipitation can be a significant parameter to consider. However, its relevance to landslide has to be evaluated in relation to classical methods (Van Asch et al., 1999). Although the appropriateness of using the recharge to better characterise the precipitation–displacement relationship is demonstrated in previous studies, the parameters used are rarely described and a state of uncertainty remains about the methods implemented (Maquaire, 2000; Binet et al., 2007; Zizioli et al., 2013; Padilla et al., 2014).

Although the method proposed in this study has not been yet tested at other sites, there are several arguments which suggest its applicability to other sites. Firstly, the FAO Penman–Monteith method used in this study is used worldwide as the evapotranspiration method standard (Allen et al., 1998; Shahidian et al., 2012). Several reduced-set evapotranspiration methods have been developed locally and many of them can be calibrated against reference method in other contexts (Hargreaves and Allen, 2003; Yoder et al., 2005; Alkaeed et al., 2006; Igbadun et al., 2006; Trajkovic, 2007; Alexandris et al., 2008; López-Moreno et al., 2009; Sivaprakasam et al., 2011; Tabari and Taleae, 2011; Shahidian et al., 2012; Tabari et al., 2013). Otherwise, Penman–Monteith reduced-set or Hargreaves–Samani methods are recommended (Allen et al., 1998).

Rainfall-triggered deep-seated landslides

A. Vallet et al.

[Title Page](#)

[Abstract](#)

[Introduction](#)

[Conclusions](#)

[References](#)

[Tables](#)

[Figures](#)



[Back](#)

[Close](#)

[Full Screen / Esc](#)

[Printer-friendly Version](#)

[Interactive Discussion](#)



**Rainfall-triggered
deep-seated
landslides**

A. Vallet et al.

[Title Page](#)[Abstract](#)[Introduction](#)[Conclusions](#)[References](#)[Tables](#)[Figures](#)[Back](#)[Close](#)[Full Screen / Esc](#)[Printer-friendly Version](#)[Interactive Discussion](#)

A number of reduced-set solar radiation methods have been developed and can be applied worldwide if locally calibrated, allowing estimation of vegetation evapotranspiration with temperature alone (Allen et al., 1998; Almorox, 2011). Recharge area parameters can be estimated locally or with local or global literature reference values according to land use. The use of global values will increase recharge estimation uncertainties. However, the implementation of a sensitivity analysis allows a refinement of recharge area parameters, in order to compensate for the lack of site-specific data. Pachepsky and Rawls (2004) have developed pedotransfer functions to estimate SAWC for different regions of the world. Runoff coefficients from the widely used rational method can be applied, as well as most of the runoff coefficients from the literature (McCuen, 2005; Musy and Higy, 2011). In addition, pedotransfer functions can also be used for runoff estimation. Finally, vegetation coefficients are available from local surveys (Gochis and Cuenca, 2000; Verstraeten et al., 2005; Hou et al., 2010), but can also be found in the literature for many species (Allen et al., 1998).

5 Conclusion and perspectives

This study demonstrates that the performance of landslide displacement data correlation with rainfall is significantly enhanced using recharge, compared to results obtained with precipitation. Most landslide sites include weather stations with limited meteorological datasets. A workflow method is developed to compute recharge on a daily interval, requiring only temperature and rainfall as inputs. Two solar radiation (R_S) methods and five commonly used reference vegetation evapotranspiration (ET_0) reduced-set methods are tested at the Séchilienne site. However, the method is developed to be as universal as possible in order to be applied to other landslides. SAWC, vegetation coefficient and runoff coefficient are estimated at the recharge area scale with a GIS composite method, and are refined with a sensitivity analysis.

For the Séchilienne landslide, the performances of all R_S tested methods are similar once they are calibrated. The five ET_0 methods tested show acceptable to very good

performance. Penman–Monteith evapotranspiration shows the best performance, and is used for recharge computation. A sensitivity analysis allows definition of a bracketed estimation of SAWC (from 75 to 115 mm) and of surface runoff (from 9 to 13.9%). A vegetation factor is estimated from 0.777 to 0.955.

5 The sensitivity analysis appears to be an appropriate alternative to estimate or to refine soil–water balance parameters of the recharge area, especially in the case of insufficient field investigations or in the absence of the necessary spatial dataset. For the Séchilienne site, temperature is missing and so has to be accurately estimated. Temperature estimation brings the greatest uncertainty in the estimation of ET_0 . Fortunately, temperature is commonly measured at weather stations near landslides.

10 The use of recharge improves the relationship between landslide displacement and rainfall signal. The proposed method for estimation of the recharge is developed in order to be sufficiently simple for use by any non-hydro specialist. The proposed method also enables the reconstruction of retrospective time series for sites recently equipped with weather stations designed to measure a full set of parameters. This method can be adapted to any other scientific study attempting to correlate time series signals with recharge. A further step will be to account for spatial and temporal variability of precipitation and recharge area properties, which will provide a better estimation of the recharge (i.e. for water budget computation).

20 In addition, taking into account recharge can assist in determining a warning rainfall threshold for Séchilienne slope movements. To our knowledge, no attempt has led to a successful determination of rainfall threshold for deep-seated landslides (Zizioli et al., 2013). Finally, an accurate estimation of the recharge will allow to better characterise the relationship between water and displacement. This would enable to determine the influence of groundwater on the seasonal variations of destabilisation (detrended displacement) and multi-annual trend behaviour. Such an understanding will be of great benefit for instance in the framework of global climate change.

HESSD

11, 6343–6403, 2014

Rainfall-triggered deep-seated landslides

A. Vallet et al.

[Title Page](#)

[Abstract](#)

[Introduction](#)

[Conclusions](#)

[References](#)

[Tables](#)

[Figures](#)



[Back](#)

[Close](#)

[Full Screen / Esc](#)

[Printer-friendly Version](#)

[Interactive Discussion](#)



Appendix A: Equations for evapotranspiration and solar radiation methods

A1 Solar radiation (R_S)

The solar radiation BCR_S obtained from the Bristow–Campbell method:

$$BCR_S = A_{BC}R_a \left[1 - \exp \left(-B_{BC}(\alpha \Delta T)^{C_{BC}} \right) \right] \quad \text{with } \Delta T_{BC} = T_{\max(j)} - \frac{T_{\min(j)} + T_{\min(j+1)}}{2} \quad (A1)$$

5 The solar radiation HSR_S obtained from the Hargreaves–Samani method:

$$HSR_S = A_{HS}R_a(\Delta T_{HS})^{B_{HS}} \quad \text{with } \Delta T_{HS} = T_{\max(j)} - T_{\min(j)} \quad (A2)$$

where: j is for the current day and $j + 1$ is for the following day, A_{BC} , B_{BC} , C_{BC} are the Bristow–Campbell empirical coefficients (no default values), A_{HS} , B_{HS} are the Hargreaves–Samani empirical coefficients ($A_{HS} = 0.16$ and $B_{HS} = 0.5$).

10 R_S can also be calculated with the Angström formula using sunshine duration data recorded at a weather station (FAO-56 guidelines, Allen et al., 1998):

$$R_S = \left(a_s + b_s \frac{n}{N} \right) R_a \quad (A3)$$

where: $a_s + b_s$ is fraction of extraterrestrial solar radiation reaching the earth on clear days. By default, $a_s = 0.25$ and $b_s = 0.5$ (without calibration).

15 A2 Reference vegetation evapotranspiration (ET_0)

The reference vegetation evapotranspiration FAO-56 PM ET_0 obtained from the Penman–Monteith method modified form from the FAO paper number 56:

$$FAO-56 \text{ PM}ET_0 = \frac{0.408\Delta(R_n - G) + \gamma \frac{900}{T_{\text{avg}} + 273} u_2 (e_s - e_a)}{\Delta + \gamma(1 + 0.34u_2)} \quad (A4)$$

6375

HESSD

11, 6343–6403, 2014

Rainfall-triggered
deep-seated
landslides

A. Vallet et al.

Title Page

Abstract

Introduction

Conclusions

References

Tables

Figures

⏪

⏩

◀

▶

Back

Close

Full Screen / Esc

Printer-friendly Version

Interactive Discussion



The reference vegetation evapotranspiration $HS ET_0$ obtained from the Hargreaves–Samani method:

$$HS ET_0 = 0.0135 \cdot 0.408 R_S (T_{avg} + 17.8) \quad (A5)$$

The unit conversion factor 0.408 was added to the original formula in order to compute ET_0 in $mm \text{ day}^{-1}$ with R_S in $MJ \text{ m}^{-2} \text{ day}^{-1}$.

The reference vegetation evapotranspiration $Turc ET_0$ obtained from the Turc method:

$$\text{For } RH > 50\%, \quad Turc ET_0 = 0.01333 \frac{T_{avg}}{T_{avg} + 15} (23.9001 R_S + 50) \quad (A6)$$

$$\text{For } RH < 50\%, \quad Turc ET_0 = 0.01333 \frac{T_{avg}}{T_{avg} + 15} (23.9001 R_S + 50) \left(1 + \frac{50 - RH}{70} \right) \quad (A7)$$

For the Séchillienne landslide, the Eq. (A6) was preferred to Eq. (A7) because of an average relative humidity (RH) of the nearby mountain weather stations greater than 50% (Chamrousse, 70%; Saint-Michel-Maur, 66%; Saint-Jean-Saint-Nicolas, 66%).

The reference vegetation evapotranspiration $PT ET_0$ obtained from the Priestley–Taylor method:

$$PT ET_0 = 1.26 \frac{\Delta}{\Delta + \gamma} (R_n - G) \quad (A8)$$

The reference vegetation evapotranspiration $M ET_0$ obtained from the Makkink method:

$$M ET_0 = 0.61 \frac{\Delta}{(\Delta + \gamma)} \frac{R_S}{2.45} - 0.012 \quad (A9)$$

The Penman–Monteith reduced-set method which allows to calculate the reference vegetation evapotranspiration $PM_{red} ET_0$ is identical to the PM FAO-56 method

6376

**Rainfall-triggered
deep-seated
landslides**

A. Vallet et al.

Title Page

Abstract

Introduction

Conclusions

References

Tables

Figures

⏪

⏩

◀

▶

Back

Close

Full Screen / Esc

Printer-friendly Version

Interactive Discussion



(Eq. A12) but humidity and wind speed are estimated according to FAO-56 guidelines (Allen et al., 1998). The actual vapour pressure is estimated with the Eq. (A10).

$$e_a = e^0(T_{\min}) = 0.611 \exp\left(\frac{17.27T_{\min}}{T_{\min} + 237.3}\right) \quad (\text{A10})$$

In the case of the Séchilienne landslide, the wind speed was fixed at 1.5 m s^{-1} at 2 m height (2 m s^{-1} by default), which is the daily average of the nearby mountain weather stations (Chamrousse, 2.33 m s^{-1} ; Saint-Michel-Maur, 0.95 m s^{-1} ; Saint-Jean-Saint-Nicolas, 1.26 m s^{-1}).

Appendix B: Temperature estimation at the Mont-Sec weather station

B1 Method

The decrease in air density with elevation leads to a decrease in air temperature known as the lapse rate (Jacobson, 2005). A commonly used value of this rate is $-6.5^\circ\text{C}/1000 \text{ m}$. The air temperature can thus be related to elevation. In order to compute a local air temperature gradient, two weather stations surrounding the Séchilienne site were used (weather stations of Luitel and La Mure). The Luitel station is located on the Séchilienne massif whereas the La Mure station is located about 18 km from the landslide. Both stations have weather conditions similar to the Séchilienne recharge area. Although temperature estimation from the Luitel station would probably be more accurate, in order to maximize common interval lengths of temperature with displacement record from 1994 to 2012, the La Mure station with record from 1992 to 2012 was selected as a reference to estimate temperature at Mont-Sec.

The local air temperature gradient in relation to elevation is defined by Equation (B1). The La Mure station temperatures (minimum and maximum) are used to estimate the temperatures at Luitel in relation to elevation, over their common recording period. A linear regression between temperature measured at La Mure and Luitel was performed to

determine the a and b coefficients. The b coefficient, which gather together the lapse rate (λ) and the elevation difference, was then divided by the elevation difference of the two stations used for the calibration.

$$T_{(\text{Station})} = aT_{(\text{Mure})} + b = aT_{(\text{Mure})} + \lambda \text{Diff}_{\text{elevation}} \quad (\text{B1})$$

with $\text{Diff}_{\text{elevation}} = \text{Elevation}_{\text{Mure}} - \text{Elevation}_{\text{Station}}$

where: a and b = regional calibration coefficients, T = temperature minimum or maximum [$^{\circ}\text{C}$], λ = temperature lapse rate [$^{\circ}\text{C m}^{-1}$], $\text{Diff}_{\text{elevation}}$ = difference of elevation between two weather stations [m], Elevation = weather station elevation [m a.s.l.], Station = target station (Luitel for the calibration, Mont-Sec for computation).

B2 Results

The estimation of the local air temperature gradient shows a very good performance with R^2 equal to 0.895 (LBCI at 5% level = 0.826) and 0.916 (LBCI at 5% level = 0.850), and RE equal to 2.12 and 2.48 respectively for minimum and maximum daily temperature calibration. Equations (B2) and (B3) are used to estimate temperatures at Mont-Sec with temperatures measured at La Mure. Instead of taking the elevation of the Mont-Sec weather station (1147 m), the average elevation of recharge area (1200 m) is used, resulting in a difference of elevation with La Mure of 319 m. The recording period used for temperature calibration was from 6 July 2006 to 23 July 2012 (2193 records). This is a common data interval for the two weather stations used (La Mure, Luitel). The estimated local air temperature gradient is 0.7°C per 100 m of elevation (the average of the λ of the two following equations).

$$T_{\min(\text{Mont-Sec})} = 0.911T_{\min(\text{Mure})} - 0.0056 \times 319 \quad (\text{B2})$$

$$T_{\max(\text{Mont-Sec})} = 0.928T_{\max(\text{Mure})} - 0.0087 \times 319 \quad (\text{B3})$$

The absence of reliable temperature records at the Mont-Sec weather station increases the estimation of R_S and ET_0 uncertainty.

Rainfall-triggered
deep-seated
landslides

A. Vallet et al.

Title Page

Abstract

Introduction

Conclusions

References

Tables

Figures



Back

Close

Full Screen / Esc

Printer-friendly Version

Interactive Discussion



Acknowledgements. This research was funded by the SLAMS program (Séchilienne Land movement: Multidisciplinary Studies) of the National Research Agency (ANR). The meteorological data were provided by MétéoFrance, LTHE, ONF and CEREMA Lyon. Aerial photographs and the digital elevation model were provided by IGN. Displacement data were supplied by CEREMA Lyon. The authors acknowledge the support of Jean-Pierre Duranthon and Marie-Aurélié Chanut from the CEREMA Lyon and Jean-Paul Laurent from the LTHE. Appreciation is also given to Eric Lucot of Chrono-Environnement for his kind advises for soil log interpretation and to Patrick Giraudoux for his support to implement bootstrap test. Finally, the authors thank Peter Milmo for English and technical proof reading.

References

- Alexandris, S., Stricevic, R., and Petkovic, S.: Comparative analysis of reference evapotranspiration from the surface of rainfed grass in central Serbia, calculated with six empirical methods against the Penman–Monteith formula, *European Water*, 21/22, 17–28, 2008.
- Alfonsi, P.: Relation entre les paramètres hydrologiques et la vitesse dans les glissements de terrains, exemples de la Clapière et de Séchilienne, *Revue française de géotechnique*, 79, 3–12, 1997.
- Alkaeed, O. A., Flores, C., Jinno, K., and Tsutsumi, A.: Comparison of Several Reference Evapotranspiration Methods for Itoshima Peninsula Area, Fukuoka, Japan, *Memoirs of the Faculty of Engineering, Kyushu University*, 66, 1–14, Kyushu University, 2006.
- Allen, R. E., Pereira, L. S., Raes, D., and Smith, M.: *Crop Evapotranspiration: Guidelines for Computing Crop Water Requirements*, FAO Irrigation and Drainage paper 56, Food and Agriculture Organization of the United Nations, Rome, 1998.
- Allen, R. G., Smith, M., Pereira, L. S., and Perrier, A.: An update for the definition of reference evapotranspiration, *ICID Bulletin of the International Commission on Irrigation and Drainage*, 43, 1–34, 1994.
- Almorox, J.: Estimating global solar radiation from common meteorological data in Aranjuez, Spain, *Turkish J. Phys.*, 35, 53–64, 2011.
- Van Asch, T. W. J., Buma, J., and Van Beek, L. P. H.: A view on some hydrological triggering systems in landslides, *Geomorphology*, 30, 25–32, doi:10.1016/S0169-555X(99)00042-2, 1999.

Rainfall-triggered deep-seated landslides

A. Vallet et al.

Title Page

Abstract

Introduction

Conclusions

References

Tables

Figures



Back

Close

Full Screen / Esc

Printer-friendly Version

Interactive Discussion



Rainfall-triggered deep-seated landslides

A. Vallet et al.

[Title Page](#)

[Abstract](#)

[Introduction](#)

[Conclusions](#)

[References](#)

[Tables](#)

[Figures](#)

⏪

⏩

◀

▶

[Back](#)

[Close](#)

[Full Screen / Esc](#)

[Printer-friendly Version](#)

[Interactive Discussion](#)



- Binet, S., Mudry, J., Scavia, C., Campus, S., Bertrand, C., and Guglielmi, Y.: In situ characterization of flows in a fractured unstable slope, *Geomorphology*, 86, 193–203, doi:10.1016/j.geomorph.2006.08.013, 2007.
- 5 Bogaard, T., Guglielmi, Y., Marc, V., Emblanch, C., Bertrand, C., and Mudry, J.: Hydrogeochemistry in landslide research: a review, *B. Soc. Geol. Fr.*, 178, 113–126, doi:10.2113/gssgfbull.178.2.113, 2007.
- Bogaard, T., Maharjan, L. D., Maquaire, O., Lissak, C., and Malet, J.-P.: Identification of hydro-meteorological triggers for Villerville coastal landslide, in: *Landslide Science and Practice*, Springer, 141–145, Berlin Heidelberg, available at: http://link.springer.com/chapter/10.1007/978-3-642-31427-8_18 (last access: 2 April 2014), 2013.
- 10 Bonzanigo, L., Eberhardt, E., and Loew, S.: Hydromechanical factors controlling the creeping Campo Vallemaggia landslide, *Symposium of landslides, Causes, Impacts and Countermeasures*, Davos, Switzerland, 17–21 June 2001, 13–22, 2001.
- Bristow, K. L. and Campbell, G. S.: On the relationship between incoming solar radiation and daily maximum and minimum temperature, *Agr. Forest Meteorol.*, 31, 159–166, doi:10.1016/0168-1923(84)90017-0, 1984.
- 15 Brocca, L., Melone, F., and Moramarco, T.: Distributed rainfall–runoff modelling for flood frequency estimation and flood forecasting, *Hydrol. Process.*, 25, 2801–2813, doi:10.1002/hyp.8042, 2011.
- 20 Brocca, L., Ponziani, F., Moramarco, T., Melone, F., Berni, N., and Wagner, W.: Improving landslide forecasting using ASCAT-derived soil moisture data: a case study of the Torgiovanetto landslide in Central Italy, *Remote Sens.*, 4, 1232–1244, doi:10.3390/rs4051232, 2012.
- Bruand, A., Duval, O., and Cousin, I.: Estimation des propriétés de rétention en eau des sols à partir de la base de données SOLHYDRO?: une première proposition combinant le type d’horizon, sa texture et sa densité apparente, *Etude et Gestion des Sols*, 11, 3, 323–334, 2004.
- 25 Canuti, P., Focardi, P., and Garzonio, C.: Correlation between rainfall and landslides, *B. Eng. Geol. Environ.*, 32, 49–54, doi:10.1007/BF02594765, 1985.
- Cappa, F., Guglielmi, Y., Rutqvist, J., Tsang, C.-F., and Thoraval, A.: Hydromechanical modelling of pulse tests that measure fluid pressure and fracture normal displacement at the Coaraze Laboratory site, France, *Int. J. Rock Mech. Min.*, 43, 1062–1082, doi:10.1016/j.ijrmms.2006.03.006, 2006.
- 30

Rainfall-triggered deep-seated landslides

A. Vallet et al.

Title Page

Abstract

Introduction

Conclusions

References

Tables

Figures

⏪

⏩

◀

▶

Back

Close

Full Screen / Esc

Printer-friendly Version

Interactive Discussion



Cartier, G. and Pouget, P.: Corrélation entre la pluviométrie et les déplacements de pentes instables, European Conference on Soil Mechanics and Foundation Engineering, 9, 17–20, Dublin, 31 August–3 September 1987, available at: <http://www.crcpress.com/product/isbn/9789061917229> (last access: 2 April 2014), 1987.

5 Castellvi, F.: A new simple method for estimating monthly and daily solar radiation, Performance and comparison with other methods at Lleida (NE Spain); a semiarid climate, *Theor. Appl. Climatol.*, 69, 231–238, doi:10.1007/s007040170028, 2001.

Chernick, M. R.: *Bootstrap Methods: a Practitioner's Guide*, Wiley, Hoboken, New Jersey, 1999.

10 Chiew, F. H. S., Peel, M. C., Western, A. W., Singh, V. P., and Frevert, D.: Application and testing of the simple rainfall-runoff model SIMHYD., *Mathematical models of small watershed hydrology and applications*, 335–367, 2002.

Cordeiro, C. and Neves, M.: The Bootstrap methodology in time series forecasting, in: *Proceedings of CompStat2006*, edited by: Black, J. and White, A., Springer, 1067–1073, Rome, Italy, 28 August–1 September 2006, 2006.

15 Crozier, M. J.: *Landslides: Causes, Consequences and Environment*, Croom Helm, London, Dover, NH, 1986.

Delmas, P., Cartier, G., and Pouget, G.: Méthodes d'analyse des risques liés aux glissements de terrain, *Bulletin liaison Laboratoire Ponts et Chaussées*, 150/151, 29–38, 1987.

Droogers, P. and Allen, R. G.: Estimating reference evapotranspiration under inaccurate data conditions, *Irrig. Drain. Syst.*, 16, 33–45, doi:10.1023/A:1015508322413, 2002.

20 Duranthon, J.-P., Effendiaz, L., Memier, M., and Previtali, I.: Apport des méthodes topographiques et topométriques au suivi du versant rocheux instable des ruines de Séchillienne, *Association Française de Topographie*, 94, 31–38, 2003.

Durville, J.-L., Kasperki, J., and Duranthon, J.-P.: The Séchillienne landslide: monitoring and kinematics, *First Italian Workshop on Landslides*, Vol. 1, 174–180, Napoli, Italia, 8 June 2009, 2009.

Garel, E., Marc, V., Ruy, S., Cognard-Plancq, A.-L., Klotz, S., Emblanch, C., and Simler, R.: Large scale rainfall simulation to investigate infiltration processes in a small landslide under dry initial conditions: the Draix hillslope experiment, *Hydrol. Process.*, 26, 2171–2186, 2012.

30 Gochis, D. and Cuenca, R.: Plant Water Use and Crop Curves for Hybrid Poplars, *J. Irrig. Drain. E.-ASCE*, 126, 206–214, doi:10.1061/(ASCE)0733-9437(2000)126:4(206), 2000.

Rainfall-triggered deep-seated landslides

A. Vallet et al.

[Title Page](#)

[Abstract](#)

[Introduction](#)

[Conclusions](#)

[References](#)

[Tables](#)

[Figures](#)

[⏪](#)

[⏩](#)

[◀](#)

[▶](#)

[Back](#)

[Close](#)

[Full Screen / Esc](#)

[Printer-friendly Version](#)

[Interactive Discussion](#)



- Godt, J. W., Baum, R. L., and Chleborad, A. F.: Rainfall characteristics for shallow landsliding in Seattle, Washington, USA, *Earth Surf. Proc. Land.*, 31, 97–110, doi:10.1002/esp.1237, 2006.
- 5 Guglielmi, Y., Vengeon, J. M., Bertrand, C., Mudry, J., Follacci, J. P., and Giraud, A.: Hydrogeochemistry: an investigation tool to evaluate infiltration into large moving rock masses (case study of La Clapière and Séchilienne alpine landslides), *B. Eng. Geol. Environ.*, 61, 311–324, 2002.
- Guglielmi, Y., Cappa, F., and Binet, S.: Coupling between hydrogeology and deformation of mountainous rock slopes: insights from La Clapière area (Southern Alps, France), *CR Geosci.*, 337, 1154–1163, doi:10.1016/j.crte.2005.04.016, 2005.
- 10 Guzzetti, F., Peruccacci, S., Rossi, M., and Stark, C. P.: The rainfall intensity–duration control of shallow landslides and debris flows: an update, *Landslides*, 5, 3–17, doi:10.1007/s10346-007-0112-1, 2008.
- Hargreaves, G. H. and Allen, R. G.: History and evaluation of Hargreaves evapotranspiration equation, *J. Irrig. Drain. E.-ASCE*, 129, 53–63, doi:10.1061/(ASCE)0733-9437(2003)129:1(53), 2003.
- 15 Hargreaves, G. and Samani, Z.: Reference crop evapotranspiration from temperature, *Appl. Eng. Agric.*, 1, 96–99, 1985.
- Helmstetter, A. and Garambois, S.: Seismic monitoring of Séchilienne rockslide (French Alps): analysis of seismic signals and their correlation with rainfalls, *J. Geophys. Res.*, 115, F03016, doi:10.1029/2009JF001532, 2010.
- 20 Hong, Y., Hiura, H., Shino, K., Sassa, K., Suemine, A., Fukuoka, H., and Wang, G.: The influence of intense rainfall on the activity of large-scale crystalline schist landslides in Shikoku Island, Japan, *Landslides*, 2, 97–105, doi:10.1007/s10346-004-0043-z, 2005.
- Hou, L. G., Xiao, H. L., Si, J. H., Xiao, S. C., Zhou, M. X., and Yang, Y. G.: Evapotranspiration and crop coefficient of *Populus euphratica* Oliv forest during the growing season in the extreme arid region northwest China, *Agr. Water Manage.*, 97, 351–356, doi:10.1016/j.agwat.2009.09.022, 2010.
- 25 Igbadun, H., Mahoo, H., Tarimo, A., and Salim, B.: Performance of two temperature-based reference evapotranspiration models in the Mkoji sub-catchment in Tanzania, *Agricultural Engineering International: the CIGR Ejournal*, VIII, available at: <http://ecommons.library.cornell.edu/handle/1813/10573> (last access: 15 April 2014), 2006.
- 30

Rainfall-triggered deep-seated landslides

A. Vallet et al.

[Title Page](#)

[Abstract](#)

[Introduction](#)

[Conclusions](#)

[References](#)

[Tables](#)

[Figures](#)

[⏪](#)

[⏩](#)

[◀](#)

[▶](#)

[Back](#)

[Close](#)

[Full Screen / Esc](#)

[Printer-friendly Version](#)

[Interactive Discussion](#)



Itenfisu, D., Elliott, R. L., Allen, R. G., and Walter, I. A.: Comparison of Reference Evapotranspiration Calculations as Part of the ASCE Standardization Effort, *J. Irrig. Drain. E.-ASCE*, 129, 440–448, doi:10.1061/(ASCE)0733-9437(2003)129:6(440), 2003.

Jacobson, M. Z.: *Fundamentals of Atmospheric Modeling*, Cambridge University Press, Cambridge, UK, New York, 2005.

Jakeman, A. J., Littlewood, I. G., and Whitehead, P. G.: Computation of the instantaneous unit hydrograph and identifiable component flows with application to two small upland catchments, *J. Hydrol.*, 1, 275–300, doi:10.1016/0022-1694(90)90097-H, 1991.

Jamagne, M., Bétrémieux, R., Bégon, J. C., and Mori, A.: Quelques données sur la variabilité dans le milieu naturel de la réserve en eau des sols, *Bulletin Technique d'Information du Ministère de l'Agriculture*, 324–325, 627–641, 1977.

Jensen, M. E., Burman, R. D., and Allen, R. G.: *Evapotranspiration and Irrigation Water Requirements: a Manual*, American Society of Civil Engineers, New York, 1990.

López-Moreno, J. I., Hess, T. M., and White, S. M.: Estimation of reference evapotranspiration in a mountainous mediterranean site using the Penman–Monteith equation with limited meteorological data, *Pirineos*, 164, 7–31, 2009.

Makkink, G.: Testing the Penman formula by means of lysimeters, *Journal of the Institution of Water Engineers*, 11, 277–288, 1957.

Malet, J. P., Maquaire, O., and Vanash, T. W.: Hydrological behaviour of earthflows developed in clay-shales: investigation, concept and modelling, in: *The Occurrence and Mechanisms of Flows in Natural Slopes and Earthfills*, Patron Editore, Bologna, 175–193, 2003.

Maquaire, O.: Effects of groundwater on the Villerville-Cricqueboeuf landslides, sixteen year survey (Calvados, France), 8th Landslides International symposium, 26–30 June 2000, Cardiff, 1005–1010, 2000.

Matichard, Y. and Pouget, P.: Pluviométrie et comportement de versants instables, in: *Proceedings of the Fifth International Symposium on Landslides*, 10–15 July 1988, Lausanne, Switzerland, 725–730, 1988.

McCuen, R. H.: *Hydrologic Analysis and Design*, Pearson Prentice Hall, Upper Saddle River, NJ, 2005.

Meric, O., Garambois, S., and Orengo, Y.: Large gravitational movement monitoring using a spontaneous potential network, in: *Proc. 19th Annual Symposium on the Application of Geophysics to Engineering and Environmental Problems (SAGEEP)*, EEGS, Seattle, USA, 2–6 April 2006, 202–209, 2006.

Rainfall-triggered deep-seated landslides

A. Vallet et al.

[Title Page](#)

[Abstract](#)

[Introduction](#)

[Conclusions](#)

[References](#)

[Tables](#)

[Figures](#)

[⏪](#)

[⏩](#)

[◀](#)

[▶](#)

[Back](#)

[Close](#)

[Full Screen / Esc](#)

[Printer-friendly Version](#)

[Interactive Discussion](#)



Mudry, J. and Etievant, K.: Synthèse hydrogéologique du versant instable des Ruines de Séchilienne, Unpublished report, UMR Chrono-Environnement, University of Franche-Comté, 2007.

Musy, A. and Higy, C.: Hydrology: A Science of Nature, English Ed., CRC Press, Science Publishers, Boca Raton, FL., Enfield, N.H., 2011.

Noverraz, F., Bonnard, C., Dupraz, H., and Huguenin, L.: Grands glissements de terrain et climat, VERSINCLIM – Comportement passé, présent et futur des grands versants instables subactifs en fonction de l'évolution climatique, et évolution en continu des mouvements en profondeur, Rapport final PNR31 (Programme National de Recherche), vdf Hochschulverlag AG an der ETH Zürich, Zürich, Switzerland, 1998.

Pachepsky, Y. and Rawls, W. J.: Development of Pedotransfer Functions in Soil Hydrology, Elsevier, Amsterdam; New York, 2004.

Padilla, C., Onda, Y., Iida, T., Takahashi, S., and Uchida, T.: Characterization of the groundwater response to rainfall on a hillslope with fractured bedrock by creep deformation and its implication for the generation of deep-seated landslides on Mt. Wanitsuka, Kyushu Island, *Geomorphology*, 204, 444–458, 2014.

Patwardhan, A., Nieber, J., and Johns, E.: Recharge estimation methods, *J. Irrig. Drain. E.-ASCE*, 116, 182–193, doi:10.1061/(ASCE)0733-9437(1990)116:2(182), 1990.

Pisani, G., Castelli, M., and Scavia, C.: Hydrogeological model and hydraulic behaviour of a large landslide in the Italian Western Alps, *Nat. Hazards Earth Syst. Sci.*, 10, 2391–2406, doi:10.5194/nhess-10-2391-2010, 2010.

Ponziani, F., Pandolfo, C., Stelluti, M., Berni, N., Brocca, L., and Moramarco, T.: Assessment of rainfall thresholds and soil moisture modeling for operational hydrogeological risk prevention in the Umbria region (central Italy), *Landslides*, 9, 229–237, doi:10.1007/s10346-011-0287-3, 2012.

Priestley, C. H. B. and Taylor, R. J.: On the assessment of surface heat flux and evaporation using large-scale parameters, *Mon. Weather Rev.*, 100, 81–92, doi:10.1175/1520-0493(1972)100<0081:OTAOSH>2.3.CO;2, 1972.

Prokešová, R., Medved'ová, A., Tábořík, P., and Snopková, Z.: Towards hydrological triggering mechanisms of large deep-seated landslides, *Landslides*, 10, 239–254, doi:10.1007/s10346-012-0330-z, 2013.

HESSD

11, 6343–6403, 2014

Rainfall-triggered deep-seated landslides

A. Vallet et al.

[Title Page](#)[Abstract](#)[Introduction](#)[Conclusions](#)[References](#)[Tables](#)[Figures](#)[⏪](#)[⏩](#)[◀](#)[▶](#)[Back](#)[Close](#)[Full Screen / Esc](#)[Printer-friendly Version](#)[Interactive Discussion](#)

Rochet, L., Giraud, A., Antoine, P., and Évrard, H.: La déformation du versant sud du mont-sec dans le secteur des ruines de Séchilienne (Isère), *Bulletin of the International Association of Engineering Geology*, 50, 75–87, doi:10.1007/BF02594959, 1994.

Le Roux, O., Jongmans, D., Kasperski, J., Schwartz, S., Potherat, P., Lebrouc, V., Lagabrielle, R., and Meric, O.: Deep geophysical investigation of the large Séchilienne landslide (Western Alps, France) and calibration with geological data, *Eng. Geol.*, 120, 18–31, doi:10.1016/j.enggeo.2011.03.004, 2011.

Rutqvist, J. and Stephansson, O.: The role of hydromechanical coupling in fractured rock engineering, *Hydrogeol. J.*, 11, 7–40, doi:10.1007/s10040-002-0241-5, 2003.

Samani, Z.: Estimating solar radiation and evapotranspiration using minimum climatological data, *J. Irrig. Drain. E.-ASCE*, 126, 265–267, doi:10.1061/(ASCE)0733-9437(2000)126:4(265), 2000.

Shahidian, S., Serralheiro, R., Serrano, J., Teixeira, J., Haie, N., and Santos, F.: Hargreaves and other reduced-set methods for calculating evapotranspiration, in: *Evapotranspiration – Remote Sensing and Modeling*, edited by: Irmak, A., InTech, Rijeka, Croatia, 2012.

Sivaprakasam, S., Murugappan, A., and Mohan, S.: Modified Hargreaves equation for estimation of ETo in a hot and humid location in Tamilnadu State, India, *Int. J. Eng. Sci. Technol.*, 3, 592–600, 2011.

Stirzaker, R., Biggs, H., Roux, D., and Cilliers, P.: Requisite simplicities to help negotiate complex problems, *Ambio*, 39, 600–607, doi:10.1007/s13280-010-0075-7, 2010.

Tabari, H. and Talaee, P. H.: Local calibration of the Hargreaves and Priestley–Taylor equations for estimating reference evapotranspiration in arid and cold climates of Iran based on the Penman–Monteith model, *J. Hydrol. Eng.*, 16, 837–845, doi:10.1061/(ASCE)HE.1943-5584.0000366, 2011.

Tabari, H., Grismer, M. E., and Trajkovic, S.: Comparative analysis of 31 reference evapotranspiration methods under humid conditions, *Irrigation Sci.*, 31, 107–117, doi:10.1007/s00271-011-0295-z, 2013.

Tan, B. Q. and O’Connor, K. M.: Application of an empirical infiltration equation in the SMAR conceptual model, *J. Hydrol.*, 185, 275–295, doi:10.1016/0022-1694(95)02993-1, 1996.

Trajkovic, S.: Temperature-based approaches for estimating reference evapotranspiration, *J. Irrig. Drain. E.-ASCE*, 131, 316–323, doi:10.1061/(ASCE)0733-9437(2005)131:4(316), 2005.

Trajkovic, S.: Hargreaves versus Penman–Monteith under humid conditions, *J. Irrig. Drain. E.-ASCE*, 133, 38–42, doi:10.1061/(ASCE)0733-9437(2007)133:1(38), 2007.

Rainfall-triggered deep-seated landslides

A. Vallet et al.

[Title Page](#)

[Abstract](#)

[Introduction](#)

[Conclusions](#)

[References](#)

[Tables](#)

[Figures](#)

[⏪](#)

[⏩](#)

[◀](#)

[▶](#)

[Back](#)

[Close](#)

[Full Screen / Esc](#)

[Printer-friendly Version](#)

[Interactive Discussion](#)



Trajkovic, S. and Stojnic, V.: Effect of wind speed on accuracy of Turc method in a humid climate, *Facta universitatis – series: Architecture and Civil Engineering*, 5, 107–113, doi:10.2298/FUACE0702107T, 2007.

5 Turc, L.: Evaluation des besoins en eau d'irrigation, évapotranspiration potentielle, formule simplifiée et mise à jour, *Ann. Agron.*, 12, 13–49, 1961.

Vengeon, J. M.: Déformation et rupture des versants en terrain métamorphique anisotrope: apport de l'étude des Ruines de Séchilienne, Ph.D. thesis, Université Joseph Fourier I, Grenoble, France, 1998.

10 Verstraeten, W. W., Muys, B., Feyen, J., Veroustraete, F., Minnaert, M., Meiresonne, L., and De Schrijver, A.: Comparative analysis of the actual evapotranspiration of Flemish forest and cropland, using the soil water balance model WAVE, *Hydrol. Earth Syst. Sci.*, 9, 225–241, doi:10.5194/hess-9-225-2005, 2005.

15 Yoder, R. E., Odhiambo, L. O., and Wright, W. C.: Evaluation of methods for estimating daily reference crop evapotranspiration at a site in the humid Southeast United States, *Appl. Eng. Agric.*, 21, 197–202, 2005.

Zêzere, J. L., Trigo, R. M., and Trigo, I. F.: Shallow and deep landslides induced by rainfall in the Lisbon region (Portugal): assessment of relationships with the North Atlantic Oscillation, *Nat. Hazards Earth Syst. Sci.*, 5, 331–344, doi:10.5194/nhess-5-331-2005, 2005.

20 Zizioli, D., Meisina, C., Valentino, R., and Montrasio, L.: Comparison between different approaches to modeling shallow landslide susceptibility: a case history in Oltrepo Pavese, Northern Italy, *Nat. Hazards Earth Syst. Sci.*, 13, 559–573, doi:10.5194/nhess-13-559-2013, 2013.

Rainfall-triggered deep-seated landslides

A. Vallet et al.

Table 1. Summary of weather datasets used in this study with parameters used (•) at each location. Distance is the distance from Séchilienne landslide, R_S is the solar radiation, N is the sunshine duration, W is the wind speed, H is the humidity, T is the temperature and P is the precipitations.

Station Name	Elevation (m a.s.l.)	Distance (km)	From	To	R_S	N	W	H	T	P	Number of days with data
Saint-Jean-Saint-Nicolas	1210	55	1 Jan 2004	1 Jan 2012	•	•	•	•	•		2876
Saint-Michel-Maur	698	54	1 Jan 2004	1 Jan 2012		•	•	•	•		2864
Grenoble-Saint-Geoirs	384	51	8 Jul 2009	1 Jan 2012	•	•	•	•	•		907
Chamrousse	1730	9	12 Sep 2002	1 Mar 2012			•	•			3261
La Mure	881	18	9 Sep 1992	1 Jan 2012					•		7517
Luitel	1277	4	6 Jul 2006	23 Jul 2012						•	2193
Mont-Sec	1148	0.2	9 Sep 1992	1 Jan 2012						•	7517

Title Page

Abstract

Introduction

Conclusions

References

Tables

Figures



Back

Close

Full Screen / Esc

Printer-friendly Version

Interactive Discussion



Rainfall-triggered deep-seated landslides

A. Vallet et al.

Table 2. R_S (solar radiation) methods: calibration results and performance assessment parameters (average of three weather stations).

A , B , C and D are the calibration coefficients, α is the cloud cover adjustment factor, R^2 is the coefficient of determination of the linear regression (measured vs. estimated R_S) and RE is the relative error. $HS_{\text{mod}}R_S$ is the solar radiation calculated with the modified form of Hargreaves–Samani method. $BC_{\text{mod}}R_S$ is the solar radiation calculated with the modified form of Bristow–Campbell method.

Method	A	B	C	D	α	R^2	RE
$HS_{\text{mod}}R_S$	0.106	0.662	0.670	–	0.740	0.847	0.123
$BC_{\text{mod}}R_S$	0.669	0.010	2.056	1.733	0.790	0.864	0.119

Title Page

Abstract

Introduction

Conclusions

References

Tables

Figures

◀

▶

◀

▶

Back

Close

Full Screen / Esc

Printer-friendly Version

Interactive Discussion



Rainfall-triggered deep-seated landslides

A. Vallet et al.

Title Page

Abstract

Introduction

Conclusions

References

Tables

Figures

◀

▶

◀

▶

Back

Close

Full Screen / Esc

Printer-friendly Version

Interactive Discussion



Table 3. Calibration and performance of the reduced-set ET_0 methods relatively to the FAO-56 PM standard (Penman–Monteith method defined in the FAO-56 paper). All reduced-set ET_0 methods are detailed in Appendix A.

a , b and R^2 are the results of linear regression between FAO-56 PM ET_0 and reduced-set ET_0 , RE is the relative error.

Method	a	b	R^2	RE
HSET ₀	0.920	0.130	0.917	0.24
Turc ET ₀	0.880	0.434	0.900	0.257
PSET ₀	0.352	0.365	0.919	0.231
MET ₀	1.107	−0.018	0.910	0.246
PM _{red} ET ₀	0.994	0.013	0.932	0.221

Rainfall-triggered deep-seated landslides

A. Vallet et al.

Table 4. K_c (vegetation coefficient), SAWC (soil available water capacity) and runoff estimation for the recharge area of the Séchilienne landslide.

Geology and vegetation are the sub-area types identified and expressed in proportion of the recharge area. Average slope gradient is the slope gradient for each vegetation sub-area type identified. K_c , runoff and SAWC are the estimated values from the spatial dataset or auger holes for each sub-area type. K_c RA, SAWC RA and runoff RA are the contribution of each sub-area type relatively to sub-area surface proportion of the recharge area. Recharge area row stands for the average estimation at whole recharge area.

Geology (%)	Vegetation (%)	Average slope gradient (°)	K_c min. max.	K_c RA min. max.	Runoff (%)	Runoff RA (%)	SAWC (mm)	SAWC RA (mm)
Micaschist	3	Pasture	14.0	0.85 1	22	5.1	173	5
Sedimentary	9						100	9
Superficial formations	11						23	112
Micaschist	12	Forest	20.6	0.745 0.935	15	7.7	254	30
Sedimentary	11						81	9
Superficial formations	30						53	133
Outcrop no soil	24	24	–	–	0	0	0	0
Recharge area	100	100	–	–	–	12.8	–	106

[Title Page](#)
[Abstract](#)
[Introduction](#)
[Conclusions](#)
[References](#)
[Tables](#)
[Figures](#)
[Back](#)
[Close](#)
[Full Screen / Esc](#)
[Printer-friendly Version](#)
[Interactive Discussion](#)


Rainfall-triggered deep-seated landslides

A. Vallet et al.

Table 6. Results of the best linear correlation between precipitation or recharge and displacement records for 4 displacement stations (1101, A13, A16 and G5). Displacement column indicates basic statistics of the displacement records (1st quartile (Q1), median and 3rd quartile (Q3)). Cumulative period (n), shift factor (β) and weighting factor (α) are the terms of the Eq. (5). LBCI is the lower bound of the confidence interval. Null hypothesis NH1 test: $R_{\text{recharge}}^2 - R_{\text{precipitation}}^2$.

Extensometer	Displacement Q1/median/Q3 mm day ⁻¹	LBCI of NH1	Precipitation/recharge			R^2
			← Cumulative period (n) day	Shift factor (β) day	Weighting factor (α)	
1101	1.75/2.50/3.84	0.124	42/68	2/2	0.0714/0.0914	0.284/0.495
A13	1.18/1.75/3.41	0.145	52/82	3/2	0.1019/0.091	0.275/0.520
A16	1.94/2.98/4.39	0.163	64/76	2/2	0.1628/0.1682	0.343/0.586
G5	0.02/0.05/0.08	0.144	8/132	0/6	0.0394/0.0110	0.0006/0.243

[Title Page](#)
[Abstract](#)
[Introduction](#)
[Conclusions](#)
[References](#)
[Tables](#)
[Figures](#)
[Back](#)
[Close](#)
[Full Screen / Esc](#)
[Printer-friendly Version](#)
[Interactive Discussion](#)


Rainfall-triggered deep-seated landslides

A. Vallet et al.

Table A1. Definition of equation parameters for all evapotranspiration and solar radiation equations.

R_a	extraterrestrial solar radiation [$\text{MJ m}^{-2} \text{day}^{-1}$]
R_S	solar radiation [$\text{MJ m}^{-2} \text{day}^{-1}$]
R_n	net solar radiation [$\text{MJ m}^{-2} \text{day}^{-1}$]
N	maximum possible duration of sunshine [h]
n	actual daily duration of sunshine [h]
T_{avg}	average air temperature at 2 m height [$^{\circ}\text{C}$]
T_{min}	minimum air temperature at 2 m height [$^{\circ}\text{C}$]
T_{max}	maximum air temperature at 2 m height [$^{\circ}\text{C}$]
G	soil heat flux density [$\text{MJ m}^{-2} \text{day}^{-1}$]
γ	psychrometric constant [$\text{kPa } ^{\circ}\text{C}^{-1}$]
u_2	wind speed at 2 m height [m s^{-1}]
e_s	mean saturation vapour pressure [kPa]
e_a	actual vapour pressure [kPa]
e^0	saturation vapour pressure at the air temperature T [kPa]
Δ	slope of vapour pressure curve [$\text{kPa } ^{\circ}\text{C}^{-1}$]
RH	relative humidity [%]

The procedure for calculating these equation terms are presented in detail in the FAO-56 guidelines for computing crop water requirements (Allen et al., 1998).

Title Page

Abstract

Introduction

Conclusions

References

Tables

Figures

◀

▶

◀

▶

Back

Close

Full Screen / Esc

Printer-friendly Version

Interactive Discussion



Rainfall-triggered deep-seated landslides

A. Vallet et al.

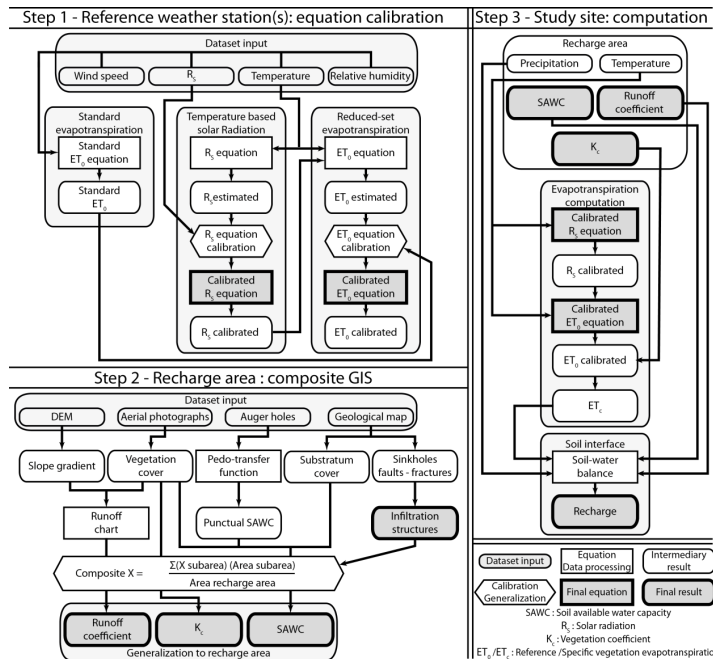


Figure 1. Recharge method workflow. Step 1: calibration of standard ET_0 (reference vegetation evapotranspiration) and R_S (solar radiation) methods. Step 2: estimation of recharge area parameters required for the soil–water balance (runoff coefficient, vegetation coefficient and SAWC) and the infiltration structures. Step 3: computation of the recharge with the soil–water balance. Reference ET_0 method matches with Penman–Monteith method defined in the FAO-56 paper and reduced-set ET_0 method with ET_0 methods requiring minimal meteorological data inputs.

Title Page

Abstract Introduction

Conclusions References

Tables Figures

◀ ▶

◀ ▶

Back Close

Full Screen / Esc

Printer-friendly Version

Interactive Discussion



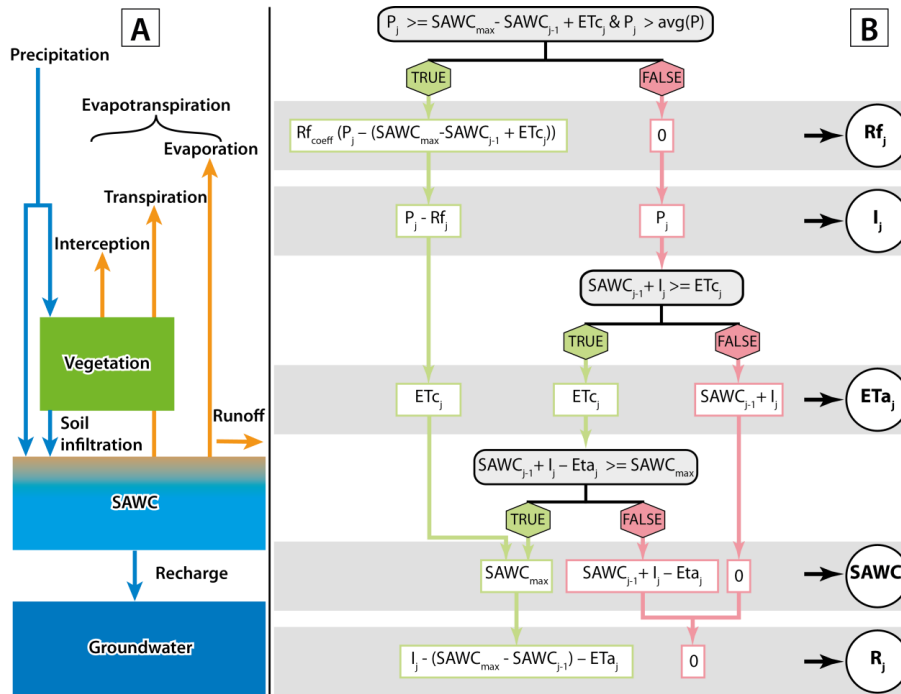


Figure 2. Soil–water balance: **(A)** soil–water balance conceptual representation and **(B)** soil–water balance diagram used for recharge computation on a daily frequency. SAWC: soil available water capacity, SAWC_{\max} : SAWC threshold (possible maximum), P : precipitation (rainfall + snow melt), $\text{avg}(P)$: precipitation average of the entire record, I : part of precipitation which infiltrate the soil, R_f : surface runoff, $R_{f_{\text{coeff}}}$: runoff coefficient, ET_c : specific vegetation evapotranspiration, ET_a : actual vegetation evapotranspiration, and R : recharge. Units: mm of water, except R_{coeff} in percent. j is the computation day and $j-1$ is the day before. TRUE and FALSE are the answers of the conditional inequality statements.

Rainfall-triggered deep-seated landslides

A. Vallet et al.

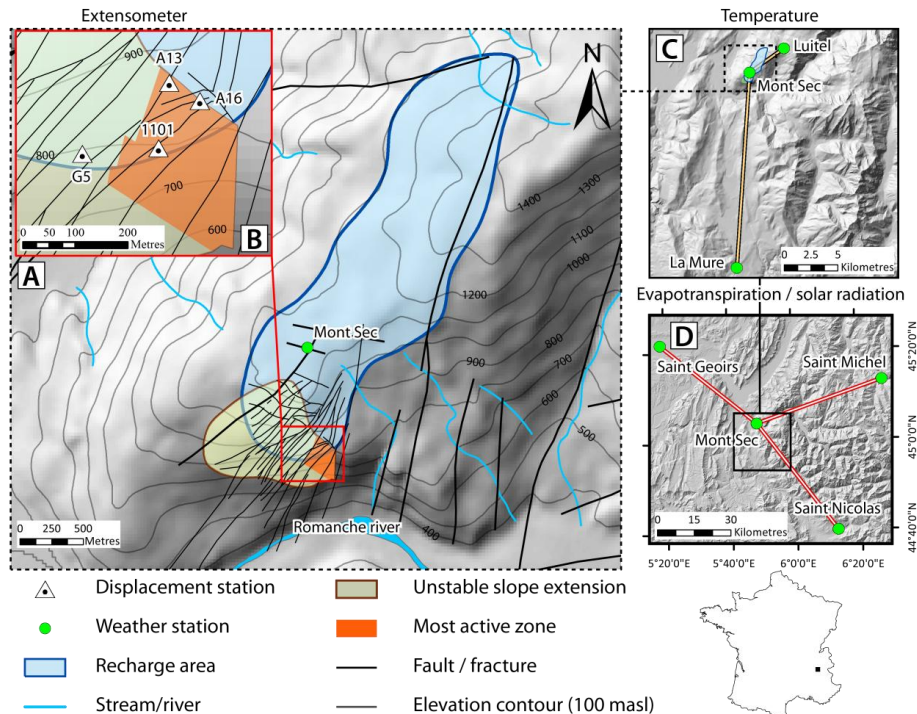


Figure 3. Location map of the studied Séchilienne landslide. **(A)** Map of the Séchilienne unstable slope and recharge area showing the Mont-Sec weather station used for recharge computation. **(B)** Enlarged map of the most active area showing displacement stations used. **(C)** Map showing the weather stations used for the temperature estimation at Mont-Sec. **(D)** Map showing the weather stations used for evapotranspiration and solar radiation method calibration.

Rainfall-triggered deep-seated landslides

A. Vallet et al.

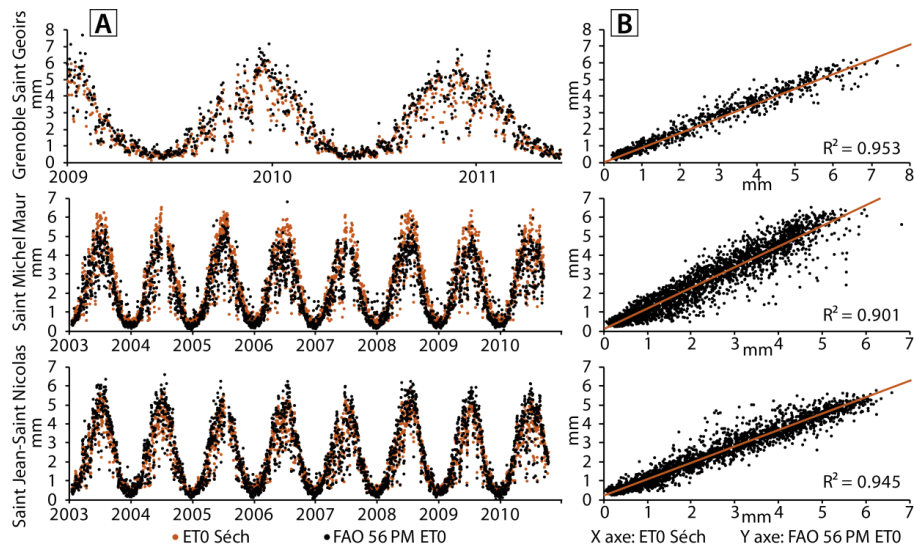


Figure 4. ET₀ (reference vegetation evapotranspiration) regional calibration results at the three reference weather stations (Grenoble-Saint-Geoirs, Saint-Jean-Saint-Nicolas, Saint-Michel-Maur). **(A)** ET₀Sé_{ch} and FAO-56 PMET₀ as a function of time. **(B)** linear regression between ET₀Sé_{ch} (x axis) and FAO-56 PMET₀ (y axis). FAO-56 PMET₀ stands for ET₀ computed with Penman–Monteith method defined in the FAO-56 paper. ET₀Sé_{ch} stands for ET₀ computed with the combination of calibrated ET₀ Penman–Monteith reduced-set method and R_S (solar radiation) modified Bristow–Campbell method.

Title Page

Abstract

Introduction

Conclusions

References

Tables

Figures

⏪

⏩

◀

▶

Back

Close

Full Screen / Esc

Printer-friendly Version

Interactive Discussion



Rainfall-triggered deep-seated landslides

A. Vallet et al.

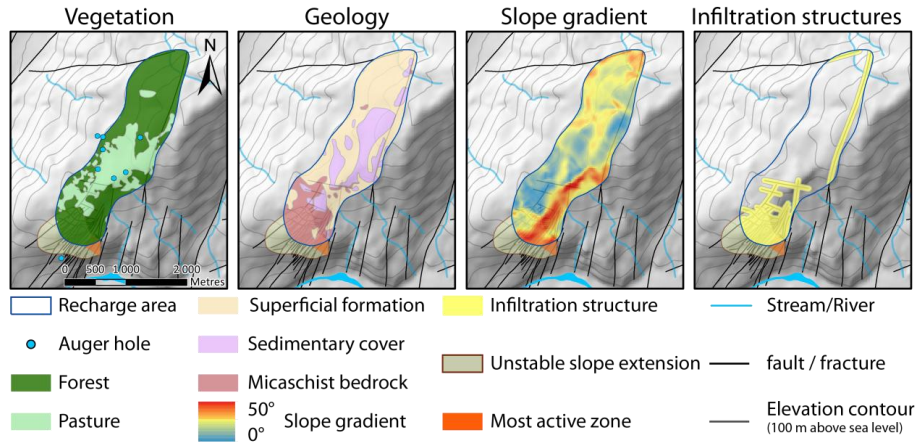


Figure 5. Interpreted spatial dataset used for the estimation of recharge area parameters.

[Title Page](#)

[Abstract](#) [Introduction](#)

[Conclusions](#) [References](#)

[Tables](#) [Figures](#)

[⏪](#) [⏩](#)

[⏴](#) [⏵](#)

[Back](#) [Close](#)

[Full Screen / Esc](#)

[Printer-friendly Version](#)

[Interactive Discussion](#)



Rainfall-triggered
deep-seated
landslides

A. Vallet et al.

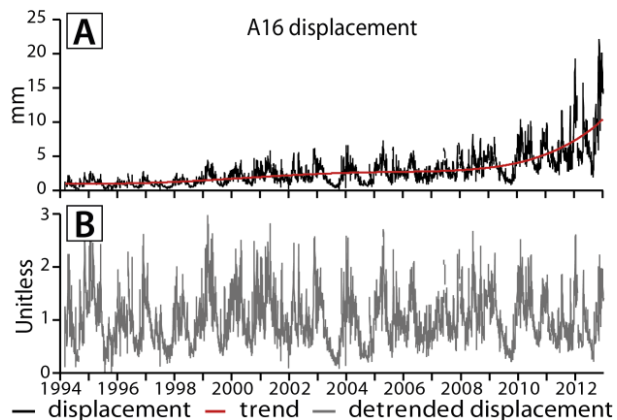


Figure 6. Trend removal of A16 extensometer displacement data with **(A)**: A16 displacement data and the fourth order polynomial curve fitting considered as the displacement trend; **(B)**: A16 detrended data (unitless) which correspond to A16 displacement data for which the trend was removed by a multiplicative method.

[Title Page](#)[Abstract](#)[Introduction](#)[Conclusions](#)[References](#)[Tables](#)[Figures](#)[⏪](#)[⏩](#)[◀](#)[▶](#)[Back](#)[Close](#)[Full Screen / Esc](#)[Printer-friendly Version](#)[Interactive Discussion](#)

Rainfall-triggered
deep-seated
landslides

A. Vallet et al.

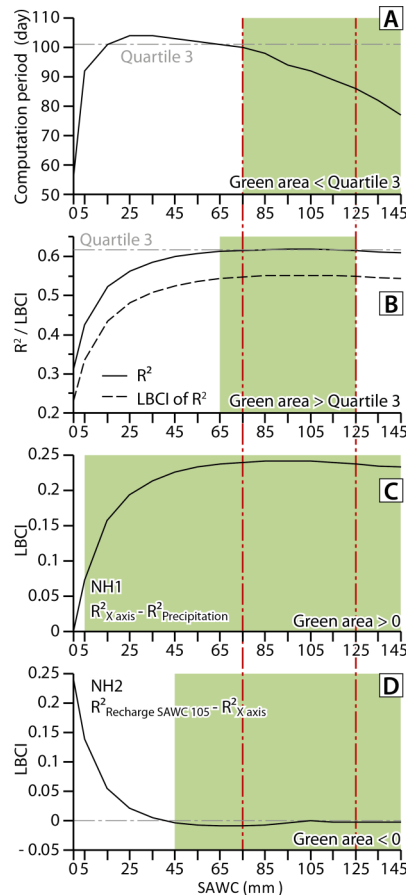


Figure 7. Results of the sensitivity analysis relative to SAWC (soil available water capacity) for **(A)** the computation period, **(B)** the R^2 and the LBCI of R^2 , **(C)** the LBCI of the null hypothesis NH1 and **(D)** the LBCI of the null hypothesis NH2. LBCI is the lower bound of the confidence interval.

Title Page

Abstract

Introduction

Conclusions

References

Tables

Figures

◀

▶

◀

▶

Back

Close

Full Screen / Esc

Printer-friendly Version

Interactive Discussion



Rainfall-triggered deep-seated landslides

A. Vallet et al.

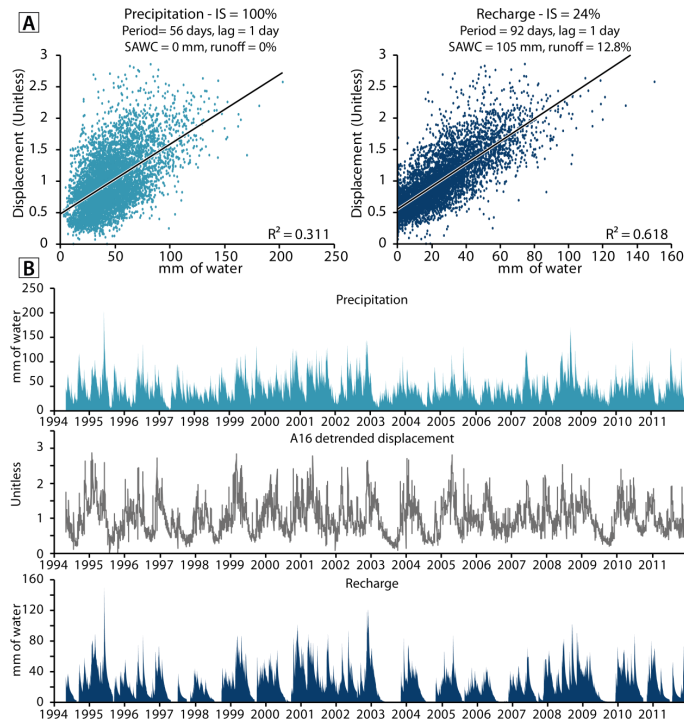


Figure 8. Best linear correlation for precipitation and recharge (IS: infiltration structures, SAWC: soil available water capacity). **(A)** Linear regression between precipitation/recharge and A16 detrended displacement as a function of time. **(B)** Correlation between precipitation/recharge and A16 detrended displacement relatively to time as a function of time.

Rainfall-triggered deep-seated landslides

A. Vallet et al.

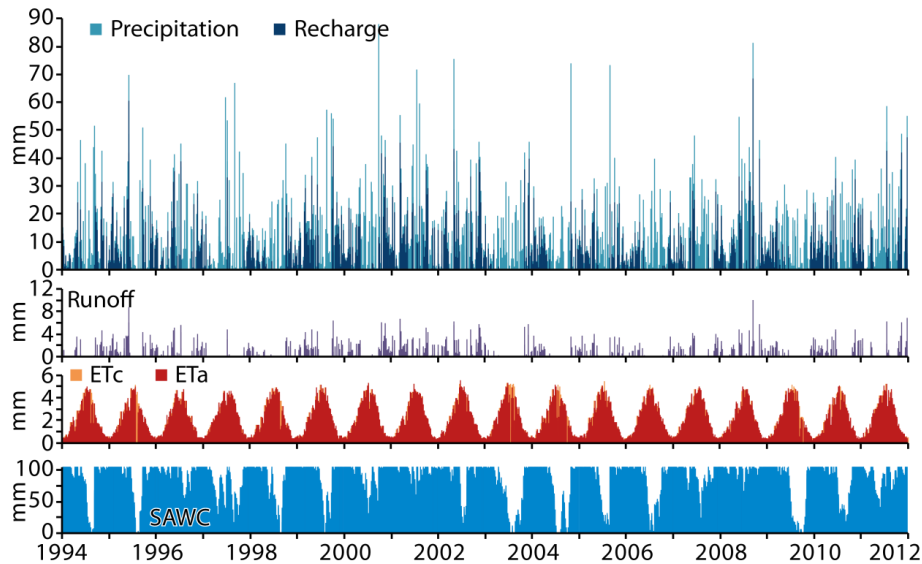


Figure 9. Recharge computation at Séchilienne with an SAWC of 105 mm and a runoff coefficient of 12.8 %. ET_c : specific vegetation evapotranspiration; ET_a : actual vegetation evapotranspiration, SAWC: soil available water capacity.

Title Page

Abstract

Introduction

Conclusions

References

Tables

Figures

◀

▶

◀

▶

Back

Close

Full Screen / Esc

Printer-friendly Version

Interactive Discussion



Rainfall-triggered deep-seated landslides

A. Vallet et al.

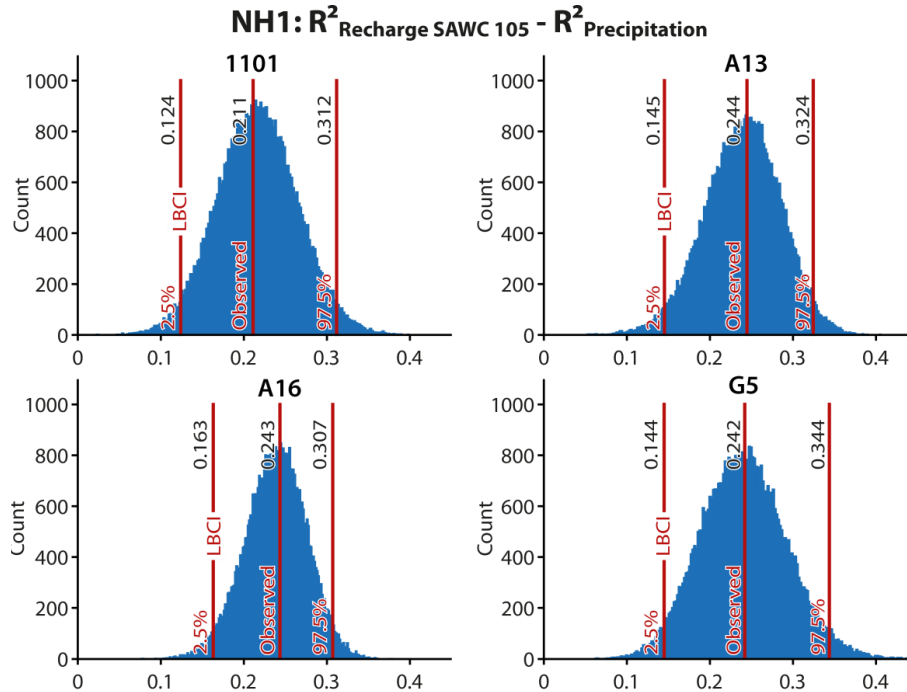


Figure 10. Bootstrap distribution of null hypothesis NH1 test for four displacement recording stations. LBCI is the lower bound of the confidence interval. Null hypothesis NH1 test: $R^2_{recharge} - R^2_{precipitation}$.

Discussion Paper | Discussion Paper | Discussion Paper | Discussion Paper | Discussion Paper

Title Page

Abstract

Introduction

Conclusions

References

Tables

Figures



Back

Close

Full Screen / Esc

Printer-friendly Version

Interactive Discussion

